UC Berkeley
UC Berkeley Previously Published Works

Title

Retinoic Acid Induces Hyperactivity, and Blocking Its Receptor Unmasks Light Responses and Augments Vision in Retinal Degeneration

Permalink

https://escholarship.org/uc/item/5j18478m

Journal

Neuron, 102(3)

ISSN

0896-6273

Authors

Telias, Michael
Denlinger, Bristol
Helft, Zachary
et al.

Publication Date

2019-05-01

DOI

10.1016/j.neuron.2019.02.015

Peer reviewed

Retinoic acid is the trigger for neural hyperactivity in retinal degeneration and blocking its receptor unmasks light responses and augments vision

Michael Telias[1,†], **Bristol Denlinger**[1,†], **Zachary Helft**[1,2,†], **Casey Thornton**[1], **Billie Beckwith-Cohen**[1,2], and **Richard H. Kramer**[1,2,*]

[1]Department of Molecular and Cell Biology, University of California, Berkeley, CA 94720, USA

[2]Vision Science Graduate Group, University of California, Berkeley, CA 94720, USA.

Summary

Light responses are initiated in photoreceptors, processed by interneurons, and synaptically transmitted to retinal ganglion cells (RGCs), which send information to the brain. Retinitis pigmentosa (RP) is a blinding disease caused by photoreceptor degeneration, depriving downstream neurons of light-sensitive input. Photoreceptor degeneration also triggers hyperactive firing of RGCs, obscuring light responses initiated by surviving photoreceptors. Here we show that retinoic acid (RA), signaling through its receptor (RAR), is the trigger for hyperactivity. A genetically-encoded reporter shows elevated RAR signaling in degenerated retinas from murine RP models. Enhancing RAR signaling in healthy retinas mimics the pathophysiology of degenerating retinas. Drug inhibition of RAR reduces hyperactivity in degenerating retinas and unmasks light responses in RGCs. Gene therapy inhibition of RAR increases innate and learned light-elicited behaviors in vision-impaired mice. Identification of RAR as the trigger for hyperactivity presents a degeneration-dependent therapeutic target for enhancing low-level vision in RP and other blinding disorders.

eTOC Blurb

Photoreceptor degeneration causes blindness, but hyperactivity of downstream neurons may obscure retinal signaling to the brain before all photoreceptors die. Here we identify the chemical

---

trigger of hyperactivity and show that blocking its receptor augments light responses in vision-impaired mice.

Introduction

Retinitis Pigmentosa (RP) is an inherited blinding disease caused by the loss of rod and cone photoreceptors. RP progresses slowly, with retinal light responses and visual acuity declining over years or decades after the initial diagnosis. Retinal ganglion cells (RGCs) maintain synaptic connectivity with the brain (Mazzoni et al., 2008; Medeiros and Curcio, 2001), making them a potential substrate for artificial vision restoration by optoelectronics (Humayun et al., 2012), optogenetics (Bi et al., 2006), or optopharmacology (Polosukhina et al., 2012; Tochitsky et al., 2014). However, because these technologies supplant light responses initiated by any residual rods and cones, they are only appropriate for end-stage degenerative disease. Hence there is an unmet need for treatment strategies that enhance, rather than replace, retinal light responses.

Even though downstream retinal neurons survive, their physiology and morphology gradually change (Marc and Jones, 2003; Marc et al., 2003). Months after the photoreceptors die, new dendritic branches appear in several types of retinal neurons and even later, cell body position begins to change in mouse, rat, and rabbit models of RP, mirroring events that occur over years in advanced human RP (Anderson et al., 2016; Jones et al., 2016; O'Brien et al., 2014; Phillips et al., 2010). A critical part of this process is that RGCs become hyperactive. Since visual stimuli are encoded by the spike patterns of RGCs, increased background firing reduces information transfer to the brain, degrading visual sensitivity. RGC hyperactivity has been attributed to increased excitatory synaptic drive (Margolis et al., 2008; Stasheff, 2008), but a large component remains after blocking chemical synaptic transmission (Borowska et al.,2011; Sekirnjak et al., 2011; Trenholm et al., 2012; Yee et al., 2012). Therefore, hyperactivity of RGCs must be the result of a change in voltage-gated channels intrinsicto RGCs (Tochitsky et al., 2016; Tochitsky et al., 2014) and/or increased electrical coupling between inner retinal neurons and RGCs (Choi et al., 2014; Ivanova et al., 2016; Toychiev et al., 2013).

While stereotypical pathophysiological events occur across mammalian species (Humphries et al., 1997; Jones et al., 2016; Marc and Jones, 2003), the signal that tells downstream neurons that the photoreceptors are degenerating is unknown. Our goal in this study was to identify this signal and ask whether blocking it can reverse pathophysiological changes, thereby improving visual sensitivity. In principle, several types of signals might induce remodeling. Perhaps death of photoreceptors leads to a decrease in a light-dependent synaptic signal, such as glutamate-induced Ca^{+2} influx, which might act as a suppressor of remodeling in healthy retina (Marc et al., 2003). Inconsistent with this idea, mice with mutations that eliminate phototransduction without causing degeneration, show no pathophysiology (Tochitsky et al., 2014). Perhaps photoreceptor death increases an inducer of remodeling. Retinoic acid (RA) has been implicated in triggering new dendritic growth in the outer retina after light-induced damage (Innocenti et al., 2004; Lin et al., 2012), leading us to ask whether it might also serve as the trigger for pathophysiological remodeling in RP.

RA is a transcriptional regulator that plays crucial roles in early embryonic development and differentiation (Conlon and Rossant, 1992; Duester, 2008; Kam et al., 2012). RA can also serve as a neural signal in adulthood, mediating synaptic plasticity in cortex and hippocampus (Chen et al., 2014; McCaffery et al., 2006; Mey and McCaffery, 2004). RA is derived from retinaldehyde (RAL), the chromophore for opsins. The loss of outer segments eliminates most opsin from the retina, perhaps allowing increased biosynthesis of RA. If RA is the trigger for RGC hyperactivity, treatments that interfere with RA synthesis or signal transduction should prevent or reverse remodeling, confirming that RA is necessary. Treatments that enhance RA signaling should mimic pathophysiological changes, confirming that RA is sufficient. A reporter of RA-induced transcription should reveal whether RA signal transduction is heightened during retinal degeneration. Finally, interventions that prevent RA signaling should reverse hyperactivity, thereby improving impaired vision.

Results

Photoreceptor degeneration leads to RGC hyperactivity

As a starting point, we measured spontaneous RGC firing in healthy retinas from wild-type (WT) mice and degenerated retina from slowly degenerating *rd10* mice and rapidly degenerating *rd1* mice. Multielectrode array (MEA) recordings from isolated *rd10* retinas show that the rise of spontaneous RGC activity correlates with the loss of light responses (Figure 1A and 1B), as shown previously (Stasheff et al., 2011). Before the onset of photoreceptor degeneration (P14), spontaneous activity in darkness was low (<1 Hz) and light-elicited firing was robust. Partway through the progression of degeneration (P28), spontaneous activity increased to 3 Hz, while light responses were reduced by ~50%. After degeneration was complete (P60), spontaneous activity increased by 6-fold, whereas light responses were undetectable. In the *rd1* mouse, photoreceptors death occurs early (P10–14), and RGCs become hyperactive as compared to WT (Figure 1C). By P60, rd1-RGCs fire at ~6 Hz (Figure 1D), similar to rd10-RGCs, but 6-fold-faster than WT-RGCs. Based on these results, all following experiments using *rd1* mice were conducted at P60–120 (i.e., 2–4 months of age, after PR degeneration is complete), and experiments using rd10 mice were conducted at P30–60 (i.e., 1–2 months of age, midpoint of PR degeneration). In all cases, WT mice used for controls were age-matched (see also STAR Methods)

To assess the component of hyperactivity that is independent of chemical synaptic input, we blocked synaptic transmission with a mixture of neurotransmitter receptor blockers (see STAR Methods). Light-responses in RGCs and spontaneous excitatory postsynaptic currents (Figure S1A and S1B) were eliminated in this solution. However, the spontaneous firing of RGCs was unaffected in all three strains (Figure 1D, Table S1), and remained 5–6-fold faster in *rd1* and *rd10* as compared to WT, indicating that none of the hyperactivity is a consequence of chemical synaptic transmission (Borowska et al., 2011; Sekirnjak et al., 2011; Trenholm et al., 2012; Yee et al., 2012). We found that photoreceptor degeneration leads to an increase in the activity of excitatory ion channels intrinsic to RGCs (Tochitsky et al., 2014). Degeneration leads to activation of gap junctional proteins that couple RGCs to amacrine cells (Choi et al., 2014; Ivanova et al., 2016; Toychiev et al., 2013). Gap junction

uncoupling reduces but does not eliminate hyperactivity (Barrett et al., 2015; Eleftheriou et al., 2017; Toychiev et al., 2013). Hence, RGC hyperactivity is a collective property of the electrically coupled network of neurons in the inner retina, but what initiates the hyperactivity is unknown.

Detecting heightened RA-induced signaling in degenerated retina with a RAR-reporter

RA signaling is mediated by nuclear retinoic acid receptors (RAR). Three different RAR isoforms exist (α, β and γ), all of them are expressed in the mammalian retina (Balmer and Blomhoff, 2002; Benbrook et al., 2014; Janssen et al., 1999; Mori et al., 2001). Upon RA binding, activated RAR binds the DNA at RA-response element (RARE) sequences, driving transcription of downstream target genes (de The et al., 1990). If RGCs are exposed to increased levels of RA in degenerated retina, RAR-dependent transcription should be increased. To test this, we developed a genetically-encoded double-fluorescent RAR-reporter for measurement of RAR-dependent transcription (Figure 2A). Multiple RARE sequences were inserted upstream of the SV40 weak promoter, driving GFP expression, while CMV was used to drive the expression of RFP (viral infection control). In HEK293 cells, transfected cells expressed RFP, but very little GFP (Figure 2B). Treatment with all-trans retinoic acid (ATRA) induced GFP expression. The increase in GFP to RFP ratio was dose- and time-dependent (Figure S2A and S2B).

Using an AAV viral vector, we injected the RAR-reporter into the vitreous of *rd1* or WT mice. Retinas were isolated 45–90 days later for imaging-based single-cell RFP and GFP fluorescence quantification in the ganglion cell layer (GCL). We compared the distribution of GFP fluorescence values across all RFP-expressing cells from WT and *rd1* retinas (Figure 2C). Median and mean GFP fluorescence values in *rd1* retina were ~4-fold higher than in WT (p<0.001, Mann-Whitney, Table S1). We also employed the RAR-reporter in *s334ter* transgenic rats, in which photoreceptor death is caused by a rhodopsin mutation identical to a subtype of human RP (Green et al., 2000) and in WT Long-Evans rats with healthy retinas. As in mice, RAR signaling was higher in degenerated rat retina than in WT retina (Figure 2D). The median and mean GFP fluorescence values in *s334ter-RGCs* were ~3-fold higher than the WT values (p<0.001, Mann-Whitney, Table S1).

These results indicate that RA-induced gene transcription is enhanced in rodent models of RP. Is RA signaling also enhanced in human RP? We compared published human transcriptome data(Mullins et al., 2012) from a sample of RP retina with a sample of non-diseased retina (Figure S3). Of all the genes represented in the retinal transcriptome dataset, 120 sequences were validated to be from RA-responsive genes, as categorized by the NIH Gene Ontology database(Harris et al., 2004). For each of these, we calculated the relative expression between the RP sample and the non-diseased sample (RP/control). Transcript levels probed by the 120 RA-responsive sequences were more than twice as abundant as the transcript levels probed by entire population of 31,108 sequences (RP/control RA-responsive genes = 3.03±0.71; RP/control for entire population = 1.44±0.014; p=0.0136, Mann-Whitney), consistent with increased RAR-transcription in human RP.

RA increases dye-permeability of RGCs

In healthy retinas, RGCs are impermeant to organic cations. In degenerated retinas, RGCs, identified by their possessing a unitary axon in the GCL, show increased membrane permeation and cytoplasmic accumulation of large molecules, including cationic fluorescent dyes and charged azobenzene photoswitches (Tochitsky et al., 2016), as a result of up-regulation and activation of P2X receptors (Browne et al., 2013; Virginio et al., 1999). To test whether RA triggers hyperpermeability, we used Yo-Pro-1, a P2X-permeant fluorescent nuclear dye. As shown previously (Tochitsky et al., 2016), Yo-Pro-1 labels a much greater percentage of *rd1-RGCs* than WT-RGCs (Figure 3A, 3B and Table S1). However, intravitreal injection of ATRA in WT retinas significantly increased the fraction of cells incorporating Yo-Pro-1 (Figure 3C). Liarozole, an inhibitor of Cyp26 (cytochrome P450 for RA-degradation), had no effect by itself, but potentiated the action of ATRA.

Retinaldehyde dehydrogenase (RALDH) converts RAL into RA (Fischer et al., 1999; Harper et al., 2015; McCaffery et al., 1992). RALDH is expressed in retinal pigmented epithelium (RPE) and retinal neurons. Injecting RAL into WT retina induced hyperpermeability, significantly increasing Yo-Pro-1 labeling above baseline and by the same amount as ATRA (Figure 3D, Table S1). Injection with the RALDH inhibitor diaethylaminobenzaldehyde (DEAB), or co-injection of RAL and DEAB, caused no change in Yo-Pro-1 labeling in WT, indicating that the hyperpermeability of RGCs is dependent on enzymatic synthesis of RA.

If the hyperpermeability induced by RA is a consequence of RAR-mediated upregulation of P2X receptors, then pharmacological blockade of RAR should reduce Yo-Pro-1 labeling. Consistent with this, co-injecting ATRA with BMS 493, an inhibitor of all RAR isoforms, eliminated the effect of ATRA on RGC permeability in WT retina (Figure 3C, Table S1). Block of P2X receptors with its antagonist TNP-ATP also prevented ATRA-induced hyperpermeability. We considered the possibility that ATRA might indirectly cause RGC hyperpermeability, for example by killing photoreceptors, which in principle might lead to RGC hyperpermeability through an RA-independent mechanism. A cytotoxic effect of ATRA on photoreceptors would be irreversible, but we find that the hyperpermeability induced by ATRA peaks within 3–7 days after injection and then disappears completely within 2 weeks (Figure S4C). Moreover, the TUNEL assay, a reliable test for cytotoxicity, showed no heightened cell death resulting from ATRA intravitreal injection (Figure S4A and S4B).

Having shown that RGC hyperpermeability can be mimicked in WT with treatments that elevate RA and activate RAR, we next asked whether hyperpermeability can be blocked in *rd1-RGCs* with treatments that interfere with RA synthesis or block RAR (Figure 3E). Intravitreal injection of DEAB or citral, both RALDH inhibitors, significantly reduced the percentage of rd1-RGCs labeled with Yo-Pro-1, as compared to vehicle-injected. Injection of BMS 493 reduced Yo-Pro-1 labeling in *rd1* to WT levels (Table S1). These results indicate that blocking RAR is more effective than blocking RA synthesis, which would spare signaling by RA that was present before drug treatment.

We also used genetic manipulations to confirm the critical role of RAR in inducing RGC hyperpermeability. We cloned into viral vectors a dominant-positive form of RARα

(**RAR$_{DP}$**, pAAV-hSyn1-VP16-RAR-RFP-WPRE) that cannot be repressed (Novitch et al., 2003); and a truncated dominant-negative form of RARα (**RAR$_{DN}$**, pAAV-hSyn1-RAR403-RFP-WPRE) that cannot be released from repression (Damm et al., 1993; Novitch et al., 2003). Both constructs employed the synapsin promoter, which drives expression exclusively in neurons. Viral-mediated gene expression began slowly (>2 weeks), but by 60 days after injection, 85% of cells in the GCL expressed RFP, a co-expression marker of viral transduction (Figure S5).

Viral expression of RAR$_{DP}$ in WT retinas dramatically increased the fraction of cells loading Yo-Pro-1 (Figure 3F), constituting 80.4±5.8% of RFP-positive cells (Figure 3G), as compared to 7.2±0.4% of all GCL cells in vehicle-injected WT control retinas without RAR$_{DP}$ treatment. The increased dye permeability was prevented by blocking of P2X receptors with TNP-ATP. Conversely, expressing RAR$_{DN}$ in *rd1* retinas led to a dramatic decrease in Yo-Pro-1 dye labeling (Figure 3F), with only 5.9±1.1% of RFP-expressing cells loading Yo-Pro-1, as compared to 26.7±1.7% of cells in vehicle-injected *rd1* control retinas without RAR$_{DP}$ treatment. It should be noted that Yo-Pro-1 labeled some non-neuronal cells, particularly vascular pericytes, whose nuclei could be identified by their small size, oblong shape, and position along blood vessels. These cells were excluded from our quantification (see STAR Methods). However, glial cells in the GCL did not exhibit RAR-induced dye labeling. Experiments utilizing a fixable analog of Yo-Pro-1 ("NucFix"), and an antibody targeted against an astrocytic marker (GFAP), revealed that none of the NucFix-labeled cells were astrocytes (Figure S6).

Taken together, these results show that RA is both necessary and sufficient for inducing hyperpermeability. Increasing RA synthesis or preventing degradation in WT retinas was sufficient to induce hyperpermeability through P2X receptors, similar to that observed in *rd1* mice. Blocking RA synthesis or RAR signal transduction in *rd1* retinas reduced permeability to a level comparable to that in WT-RGCs, demonstrating that RA and RAR-activation are necessary for pathophysiological hyperpermeability.

RA-signaling enables chemical photosensitization of RGCs

Azobenzene photoswitches are synthetic photoisomerizable molecules that can bestow light-sensitivity on neurons that express no native photoreceptor proteins and ordinarily have no intrinsic light response (Mourot et al., 2012; Mourot et al., 2011). Remarkably, photoswitch compounds affect RGCs from blind retinas, but have no effect on RGCs from healthy retinas (Tochitsky et al., 2014) across mammalian species, suggesting a common mechanism. We found that photoswitches, like Yo-Pro-1, enter RGCs through up-regulated P2X receptors (Tochitsky et al., 2016). If RA is the initiator of both processes, increasing or decreasing RA-signaling should have effects on photoswitching that parallel dye-labeling.

To test this, we carried out intravitreal injections with drugs that alter RA-signaling and, 3–7 days later, measured light responses imparted by QAQ, a photoswitch that acts on voltage-gated Na$^+$, K$^+$, and Ca^{2+}-channels found in all neurons. Light-dependent firing was quantified by calculating Photoswitch Index (PI) (Polosukhina et al., 2012). We first asked whether increasing RA-signaling in WT-RGCs could mimic the degeneration-dependent photosensitization observed in *rd1-RGCs*. Injection of WT retina with ATRA plus liarozole

enabled QAQ to elicit light-dependent firing (Figure 4A and 4B), significantly higher than its control (Figure 4C, Table S1), and similar to *rd1* retina. Neither ATRA nor liarozole alone enabled significant QAQ photosensitization. The effect of ATRA plus liarozole was blocked by TNP-ATP, and wore off within 6 weeks after injection, consistent with reversible enhancement of RA-signaling. These features, including synergy between ATRA and liarozole, block by P2X receptor antagonists, and reversibility weeks after injection, mirror the effects of RA-signaling on Yo-Pro-1 labeling, consistent with a common mechanism. Consistent with this, inhibition of RAR in *rd1* mice injected intravitreally with BMS 493, prevented QAQ photosensitization and reduced the PI to a value similar to that observed in WT (Figure 4D and 4E).

RAR inhibitors reduce hyperactivity and enhance light sensitivity in degenerating retinas

Our results indicate that RA signal transduction is necessary and sufficient for inducing degeneration-dependent hyperpermeability of RGCs, which allows otherwise impermeable dyes and photoswitches to access RGCs. However, the effects of RA could potentially expand to all other cell types in the surviving inner retina of blind mice. If RA is necessary and sufficient for inducing enhanced spontaneous activity in the inner retina, including RGCs but also potentially amacrine and bipolar cells, then blocking RA signaling should reduce pathologically-enhanced spontaneous firing in the degenerated retina. To test this, we obtained MEA recordings in saline (Figure 5A) from isolated *rd1* retina injected either with BMS 493 or with pAAV2-RAR$_{DN}$. Spontaneous firing rates were significantly lower in BMS 493- or RAR$_{DN}$-treated retina as compared to controls (Figure 5B). Hence RAR activity is necessary for hyperactivity in the inner retina.

In human RP, photoreceptors gradually degenerate. The death of cones is secondary to the death of rods, and the cell bodies of some cones can persist for years, particularly in the fovea (Milam et al., 1998). Remnant cones can generate light-responses that are reduced in sensitivity and amplitude, but not completely eliminated (Busskamp et al., 2010). However, high background firing of RGCs obscures light responses, particularly to low-intensity stimuli. Blockers of RA signaling might augment light-responses and enhance visual performance. To test this idea, we used the *rd10* mice at 6-weeks of age, when their retinas were incompletely degenerated. We injected one eye with BMS 493 and the other with vehicle, and evaluated retinal sensitivity with light flashes of varying intensity. BMS 493-treated retinas showed a transient increase in RGC firing in response to a brief flash (50ms) of dim light, whereas vehicle-treated retinas showed no RGC response to the same flash (Figure 6A and 6B, Kruskal-Wallis ANOVA, Dunn's post-hoc p=0.0263). The emergence of the light response was associated with a decrease in the background firing rate in darkness. BMS 493-enhanced the light response in all mice tested (Figure 6C). Measuring over a variety of intensities revealed a shift in the intensity-response curve (Figure 6D) reflecting an increase in sensitivity and peak response to light. The response threshold was lower for BMS 493-injected than for vehicle-injected eyes (0.15 mW vs 0.85 mW). Hence, inhibiting RA-signaling dramatically boosts the light-response of RGCs in partially degenerated retinas.

Inhibiting RAR with gene therapy enhances behavioral light sensitivity in vision-impaired mice

We next asked whether the increase in light sensitivity bestowed by RAR inhibition translates into increased behavioral sensitivity to light *in-vivo* (Figure 7). We injected neonatal *rd10* mice with RAR_{DN} (Figure 5, Figure S5, Methods), with the goal of inhibiting RAR before degeneration is complete, such that visual function is impaired but not entirely lost. Since intraocular injections are damaging in neonates, we used the AAV9 serotype, which can be injected into the vasculature to efficiently transduce retinal neurons early in postnatal life(Byrne et al., 2015). Light-elicited behavior was evaluated at P30–40.

First, we tested innate light-aversion in P37–39 mice (Figure 7A) using an automated double-chamber light/dark box (Methods) and quantified the time spent in each side. In darkness, mice had no preference. Illuminating one side with dim light had no effect on untreated *rd10* mice, but $rd10$-RAR_{DN} mice preferred the dark side significantly more. In 10-fold brighter light, both treated and untreated mice preferred the dark chamber. Hence, RAR_{DN} increased the light sensitivity of innate behavior in vision-impaired mice.

We next examined learned light-aversion in P33–35 *rd10* and WT mice (Figure 7B-D). Employing a shock-box (Methods), we tested whether RAR_{DN} could enhance learned aversion to visual cues of different intensities. This test was used previously to measure light-sensitivity in *rd1* mice treated with photoswitches for vision restoration(Tochitsky et al., 2014). Light-adapted *rd10,* $rd10$-RAR_{DN} and WT mice learned to associate 10-seconds-long/6000 $\mu W/cm^2$ light-flashes with 2-seconds-long/0.7 mA electric shocks. Their freezing behavior was then assessed before and after light-stimuli with increasing intensities. Individual traces for each mouse show the variability of the response (Figure 7B). As compared to WT, *rd10* mice show poor responses, which seem to be rescued by using RAR_{DN}-gene therapy. WT and $rd10$-RAR_{DN} mice were able to recall the behavior starting at the second light-flash, and maintained a consistent response for higher intensities, in spite of behavioral extinction (Figure 7C). Analysis of the slope of the response to the first and dimmest light flash was used to establish a threshold, equally applied to all mice (Figure 7D). We found that 8 out of 9 WT mice responded to the first light flash, 5/9 in *rd10* and 8/11 in $rd10$-RAR_{DN}.

The same mice were used for PCR confirmation of RAR-signaling manipulation by RAR_{DN}. At P40, mice were sacrificed, and mRNA was extracted and purified from their retinas (Figure 7E). Semi-quantitative reverse-transcriptase assay shows no change, associated with RAR_{DN}, in the transcription of *rhodopsin* and *β-actin. RARct* expression was significantly increased in $rd10$-RAR_{DN}, reflecting overexpression of the virus, and *RFP (mStrawberry)* expression was detected only in treated retinas. RAR_{DN} significantly reduced the expression of RAR-regulated genes, such as *RARβ* and *Cyp26,* demonstrating an effective downregulation of RAR-signaling.

Taking together the results in Figures 5, 6 and 7, we demonstrate that inhibition of RAR-activation effectively reduces pathophysiological hyperactivity in degenerating retinas, rescuing electrophysiological light responses *ex-vivo* and behavioral light responses *in-vivo.* These results open the possibility of using RAR as a drug and gene therapy target for

improving light responses in patients suffering from slow-progressing degenerative blindness.

Discussion

RA is the photoreceptor degeneration-dependent trigger for pathophysiological remodeling

Our evidence shows that RA is necessary and sufficient for inducing pathophysiological remodeling of the retina during the progression of photoreceptor degenerative disease. The P2X receptor-dependent hyperpermeability of RGCs, characteristic of degenerated retina, is greatly reduced with drugs that block RALDH, and eliminated with a drug that inhibits RAR. Likewise, pathophysiological changes can be induced in WT retina with agents that either directly or indirectly increase RA. Providing the retina with RA itself or with excess RAL, induces hyperpermeability, mimicking the pathophysiological state. Further supporting the hypothesis that RA is the trigger, our RAR-reporter detected enhanced RA-signaling in mouse and rat degenerated retina. RA has also been implicated in morphological remodeling of dendrites in the outer retina in a light-induced model of blindness(Lin et al., 2012). These results suggest that both fast functional changes and slower structural remodeling are triggered by RA.

The loss of photoreceptors in RP deprives downstream retinal neurons of sensory information. Sensory deprivation leads to homeostatic plasticity in neural circuits in the brain, including changes in excitatory and inhibitory synaptic strengths and in the intrinsic membrane properties of postsynaptic neurons (Turrigiano, 1999). In principle, homeostatic plasticity could contribute to degeneration-dependent RGC hyperactivity. However, studies on blind mice that have dysfunctional but intact photoreceptors, indicate that loss of light-dependent synaptic signaling alone is insufficient to trigger remodeling (Tochitsky et al., 2014), the physical loss of photoreceptors is required. Photoreceptor death in RP, Usher's syndrome, retinal detachment and AMD trigger similar remodeling events (Coblentz et al., 2003; Marc et al., 2003), consistent with a common triggering mechanism, perhaps involving RA.

Source and mechanism of action of RA in the degenerating retina

RA is synthesized from RAL by the RALDH, which is expressed ubiquitously in the retina (Fischer et al., 1999; Harper et al., 2015; McCaffery et al., 1992). RAL is produced by isoforms of retinol dehydrogenase (RDH) that are expressed only in cells exposed to the subretinal space, including photoreceptors, RPE and Muller glial cells (Parker and Crouch, 2010). Delivering excess RAL to WT retina induced the same changes as observed in WT retinas treated with ATRA or in untreated *rd1* (Fig 3,4). The effect of RAL was blocked with a RALDH inhibitor, confirming that conversion to RA is required. These results suggest that availability of RAL is limiting for the initiation of subsequent pathophysiological events. The retina contains millions of photoreceptors each with millions of opsins. Loss of photoreceptors removes an enormous molecular sink for RAL. We speculate that photoreceptor death also causes a breach in the outer limiting membrane and compromises the compartmentalization of RAL to the subretinal space. Several cell types in the

degenerated retina could convert some of the excess RAL into RA. Our RAR-reporter shows that RA-induced transcription is heightened in RGCs, demonstrating that RA reaches RGCs and activates gene transcription.

RA can signal through activation of nuclear RARs that regulate gene transcription (Balmer and Blomhoff, 2002; Benbrook et al., 2014). Alternatively, RA can signal through a non-canonical mechanism that is RAR-independent, in which RA directly binds to protein kinases and phosphatases (Aggarwal et al., 2006). However, we found that blocking the activity of RAR with BMS 493 or RAR_{DN} was sufficient to reduce hyperactivity and hyperpermeability in degenerated retina. Previously, we implicated up-regulation and activation of P2X7 receptors in hyperpermeability, and up-regulation of HCN channels in hyperactivity (Tochitsky et al., 2016; Tochitsky et al., 2014). The genes encoding P2X7 and HCN isoforms do not possess the RARE sequence in their promoter. However, RAR often operates through transcriptional cascades leading to indirect activation of genes without RARE (Balmer and Blomhoff, 2002). RAR can also signal post-transcriptionally, for example by binding to RNA granules, regulating local dendritic protein synthesis in neurons (Chen et al., 2014; Maghsoodi et al., 2008).

RGCs can be categorized by their light-response properties, and dendritic stratification pattern into ON, OFF, or ON/OFF types. Only OFF-RGCs exhibit hyperpermeability (Tochitsky et al., 2016) and hyperactivity (Margolis et al., 2008; Sekirnjak et al., 2011) as a consequence of photoreceptor degeneration. If RA is the trigger for remodeling, then OFF-RGCs must either be exposed to higher RA or they respond more vigorously to RA. The dendrites of OFF-RGCs ramify in the sublamina of the inner plexiform layer that is closest to the outer retina, which includes the degenerating photoreceptors, providing a possible basis for selective exposure RA. Alternatively, OFF-RGCs may be selectively responsive to RA by expressing a transcriptional program that is absent or different than other RGCs. Bipolar and amacrine cells also show physiological and morphological remodeling after photoreceptor degeneration. Bipolar cells sprout new dendritic branches in response to elevated RA (Lin et al., 2012). A-II amacrine cells show increased phosphorylation of connexin-36 during degeneration (Ivanova et al., 2016) enhancing electrical coupling behind spontaneous oscillations. The trigger for remodeling in these cells might also be RA, but this has not yet been investigated.

Improving low-level vision by blocking RA signal transduction

Retinal remodeling in RP is preserved across mammalian species, with stereotypical changes in physiology and morphology (Humphries et al., 1997; Jones et al., 2016; Marc and Jones, 2003; Marc et al., 2003). The fundamental defect in RP is loss of photoreceptors, but downstream retinal remodeling might greatly exacerbate vision impairment during disease progression. Hyperactive firing of RGCs masks light-elicited signals initiated by surviving photoreceptors, potentially corrupting visual information sent to the brain. An analogous situation occurs with tinnitus in hearing loss, where degeneration of cochlear hair cells leads to hyperactivity of auditory neurons (Middleton et al., 2011), interfering with the remaining sound-elicited neural signals. Separating the component of the visual deficit resulting directly from photoreceptor death from the component imposed by RGC

hyperactivity is not straightforward in humans. While non-invasive recording methods such as pattern electroretinogram can detect changes in RGC firing with rapidly changing visual stimuli (Porciatti, 2015), spontaneous RGC firing in the absence of visual stimuli cannot be detected. Unfortunately, there are no models of inherited retinal degeneration in non-human primates. However, positron emission tomography scans show increased glucose metabolism in the visual cortex of early-blind patients, attributed to elevated spontaneous neural activity (De Volder et al., 1997). Human subjects with RP have a heightened threshold for electrically-induced phosphenes, consistent with interference by spontaneous retinal activity (Delbeke et al., 2001). Directly linking human RP with enhanced RA-induced transcription is limited by the availability of retinal tissue samples with non-degraded mRNA, but the very limited data that have been collected suggest an increase in RA-responsive gene transcription (Fig. S3 and Mullins et al., 2012).

We have shown that inhibition of RAR reduces retinal hyperactivity, increases light-sensitivity, and boosts behavioral light responses in vision-impaired mice. Meclofenamic acid, an uncoupler of gap junctions, also augments RGC light responses by reducing hyperactivity (Ivanova et al., 2016; Toychiev et al., 2013), but micromolar concentrations are required and gap junctions are essential for normal retinal functioning. In contrast, RAR inhibitors act at nanomolar concentrations, and they interfere with RA-dependent transcription, a process that is largely absent in RGCs in the healthy retina. Thus, RAR inhibitory drugs should be efficacious in degenerating retinal tissue, while having minimal effects on healthy retinal tissue. Our findings open the door to the possible use of pharmacological inhibitors of RARs as a first-in-class vision-enhancing drug. A rich pharmacopoeia of RAR inhibitors has already been developed (Germain et al., 2006; Germain et al., 2009). In this study we used BMS 493, a pan-RAR inverse agonist, but RAR antagonists are also available, either with broad or narrow subunit-specificity. Our findings also suggest a gene therapy approach, utilizing AAV to deliver RAR_{DN}. By selecting a specific AAV serotype or a specific promoter, or a combination of both, a particular type of retinal neuron may be targeted for blockade of RA signal transduction (Martin et al., 2002; Trapani and Auricchio, 2018).

Even after all the photoreceptors have degenerated and light perception is absent, reducing RGC hyperactivity could still be beneficial in blind patients. Responses evoked by optoelectric (Dagnelie et al., 2017; Stronks and Dagnelie, 2014), optogenetic (Barrett et al., 2015; Bi et al., 2006), or optopharmacological (Tochitsky et al., 2018) stimulation of the degenerated retina are superimposed on the heightened background activity of RGCs, curtailing the encoding of visual images. The combination of a light-sensitive actuator with an RAR inhibitor could have a synergistic effect, boosting neural signals to more effectively restore visual function to blind patients.

STAR Methods

CONTACT FOR REAGENT AND RESOURCE SHARING

Further information and requests for resources and reagents should be directed to and will be fulfilled by the Lead Contact, Richard H. Kramer, (rhkramer@berkeley.edu).

EXPERIMENTAL MODEL AND SUBJECT DETAILS

Animals—Animals used included WT mice (C57BL/6J strain, Jackson Laboratory or Charles River), homozygous rd1 mice (CH3/Hej) (Jackson Laboratory stock #000659, RRID:IMSR_JAX:000659), homozygous rd10 mice (B6.CXB1-Pde6b^{rd10}/J) (Jackson Laboratory stock #004297, RRID:IMSR_JAX:004297), WT rats (Long Evans strain, Charles River Laboratories) and s334-ter rats (line #3, Matthew LaVail, UCSF). Male and female rats and mice were used alike. Unless stated otherwise in the results or figure legends, all mice used were 1–4 months old and all rats were 2–6 months old. Neonate *rd10* mice were used for AAV9 tail-vein injection, and tested for behavior and ex-vivo recordings at ages P30-P90. Animals were housed in a 12-hour light/dark cycle and provided with standard chow and water *ad-libitum.* No more than 6 mice were housed in one cage, and no more than 2 rats were housed in one cage. All animal use procedures were approved by the UC Berkeley Institutional Animal Care and Use Committee.

Cell Lines—HEK293T cells were routinely grown on polystyrene flasks (Nunc). Media used was Dulbecco's Modified Eagle Medium (DMEM, Thermo-Fisher), containing 10% Fetal Bovine Serum (Thermo-Fisher), 1% GlutaMAX (Gibco) and 1% penicillin-streptomycin (Sigma-Aldrich). Cells were purchased from and authenticated by the Cell Culture Facility at the Biosciences Divisional Services, University of California, Berkeley.

METHOD DETAILS

Chemicals—Chemicals were obtained from Sigma-Aldrich, Tocris Bioscience, Life Technologies, Biotium, and Santa Cruz Biotech.

Viruses

Retinoic Acid Receptor reporter: A custom-designed and synthesized AAV vector (Vigene Biosci., Maryland, USA) included a cytomegalovirus promoter (CMV) upstream to the coding sequence for the red fluorescent protein (RFP, 'mStrawberry'), followed by poly-A tail and a stop sequence. A fragment containing three repetitions of the retinoic acid response element (RARE) sequence followed by the weak promoter SV40 was sub-cloned from pGL3-RARE-luciferase (Addgene Plasmid #13458), a kind gift of the Underhill Lab (Hoffman et al., 2006). Finally, a green fluorescent protein (GFP) sequence was sub-cloned downstream to SV40, for a final construct of pAAV-CMV-RFP-stop-RARE(x3)-SV40-GFP. The presence of inverted terminal repeat sequences was confirmed by enzymatic digestion. Final titer was ~10 particles/μl.

RAR$_{DP}$ and RAR$_{DN}$.: The dominant-positive (pCIG-VP16-RARα; Addgene plasmid #16287) and dominant-negative (pCIG-RARα403-myc; Addgene plasmid #16286) form of RARα (renamed in this study RAR$_{DP}$ and RAR$_{DN}$, respectively) were a kind gift of the Jessell Lab (Novitch et al., 2003). The coding region for each was sub-cloned into a pAAV backbone under the expression of human synapsin 1 (hSyn1). The final constructs were pAAV-hSyn1-VP16-RARα-RFP-WPRE and pAAV-hSyn1-RARα403-myc-RFP-WPRE. The presence of inverted terminal repeat sequences was confirmed by enzymatic digestion. Final titer was ~10^{14} particies/μl.

Serotype: Viruses were produced either as AAV2 or AAV9 serotypes. AAV2 (Cehajic-Kapetanovic et al., 2011) was used for intravitreal injections in adult mice and rats, while AAV9 (Byrne et al., 2015) was used for tail-vein injection of P2–3 mouse neonates.

Injections

Intravitreal injections: Adult mice and rats were intravitreally injected with drugs or viruses. Before injection, animals were anesthetized with isoflurane (2%) and their pupils were dilated with tropicamide (1%) and phenylephrine (2.5%). Proparacaine (0.5%) was used as a topical analgesic. Genteal was applied under a glass coverslip to keep the cornea lubricated. An incision was made through the sclera below the ora serrata with a 30G needle. Solutions were injected into the vitreous with a blunt-ended 33G Hamilton syringe. After injection, the antibiotic tobramycin (0.3%) was applied to the eye. Final drug concentrations (after 5-fold dilution in the vitreous) were: 100 µM all-trans retinoic acid (ATRA), 100 µM liarozole (Van Wauwe et al., 1992), 20 µM diethylaminobenzaldehyde (DEAB) (Chute et al., 2006; Russo et al., 1988), 50 µM citral, 500 µM BMS 493 (Germain et al., 2009), 1 µM retinaldehyde, and vehicle comprising of $1\times$ phosphate buffered saline (PBS) containing 1% dimethyl sulfoxide (DMSO). Intravitreal injections were performed using AAV2 serotype only. WT and rd1 mice were injected with the RAR-reporter virus or the RAR_{DN} virus, at age 1–1.5 month-old. WT and s334ter rats were injected with the RAR-reporter virus at age 3–4 month-old. Final volume of injections was 1–1.5 µl for mice and 5 µl for rats.

Tail vein injections: Neonatal mice were injected via one or both tail veins at ages P2–3 with an AAV9 (Byrne et al., 2015) virus to achieve expression of the vector in the central retina. Prior to each injection, neonates were cryo-anesthetized on a latex glove placed on wet ice for 45–60 seconds and immobilized. All tail vein injections were performed with a final volume of ~7–10 µI. WT and rd1 mice were injected with the RAR-reporter virus. rd10 mice were injected with the RAR_{DN} virus.

General considerations for experimental design

Replication: Unless stated otherwise, every MEA recording, dye loading, RAR-reporter imaging and behavioral experiment was conducted only once on each individual animal, as all experiments were terminal for each individual mice.

Sample size estimation: Sample size was empirically determined in every case. As a general rule, every retina from every enucleated eye was cut in 3–4 pieces and the analysis was conducted in at least 2 pieces. If only 1 piece was available for analysis, that retina and its control were excluded from the analysis. Statistical methods as well as exclusion criteria used were described in each related section and detailed in "Quantification and Statistical Analysis."

Blinding and randomization: In MEA and dye loading experiments performed following intravitreal injections with a pharmacological agent, one eye was injected with the drug and the other with vehicle by a technician and noted as "R" or "L" in a log, alternating the order of injections between mice, using ear clips or tail markings to identify each mouse. Researchers conducting MEA and dye-loading assays (5–7 days later) were blind to the

specific treatment in each eye, and performed their tests and analysis alternating between R and L retinal pieces. The injection log and test results were compared *post-hoc.* For behavioral experiments, blinding was conducted only between rd10 mice (WT controls were always known to the researcher). In every rd10 neonate litter used for either experiment, half of the neonates were randomly selected to receive treatment (tail vein injection with RAR_{DN}) and returned to the cage with the rest of the littermates, unmarked. As adults, all mice were first ear-clipped for individual identification and then subjected to one of two behavioral tests in no specific order. At the end of the experiment mice were euthanized and their retinas were imaged for RFP fluorescence and tested for viral-driven gene expression using RNA purification and RT-PCR to determine presence/absence of the virus in the retina.

Tissue preparation—Eyes were obtained from mice and rats immediately following euthanasia. Retinas were removed and kept in saline (artificial cerebrospinal fluid) containing (in mM) 119 NaCl, 2.5 KCl, 1 KH 2 PO 4, 1.3 MgCl 2, 2.5 CaCl 2, 26.2 NaHCO 3, and 20 D-glucose, aerated with 95% O_2 / 5% CO_2 and at room temperature until recording. For imaging (Yo-Pro-1, RAR-reporter), retinal pieces were flat-mounted on filter papers with GCL side up.

Multi electrode array and patch-clamp recordings—Flat-mounted retina was placed ganglion cell layer down onto a 60-electrode Multi-Electrode Array (MEA 1060–2-BC, Multi-Channel Systems). After mounting the retina was left to dark adapt for 20 minutes under constant perfusion with oxygenated saline at 34°C. 300 μM QAQ at was applied for 30 min, followe d by a 5 min wash. A solution containing a mixture of neurotransmitter receptor blockers isolated RGCs from synaptic inputs: (in μM) 10 AP4, 40 DNQX, 30 AP5, 10 SR-95531,50 TPMPA, 10 strychnine, and 50 tubocurarine. In experiments where P2X channels were blocked, the retina in the MEA chamber, was pretreated with 100 μM TNP-ATP (Virginio et al., 1998). Extracellular spikes were high-pass filtered at 200 Hz and digitized at 20 kHz and were counted when exceeding 4 SD from the mean background voltage signal. Typically, each electrode recorded spikes from one to three individual RGCs. Principal component analysis of the spike waveforms was used for sorting spikes generated by individual cells (Offline Sorter, Plexon). Stimulation light was generated from a 100 W mercury arc lamp. Neutral density filters were used to alter the light intensity of the 50 ms light flashes. Narrow band optical filters (Chroma) were used to deliver alternating intervals of 380 nm and 500 nm for stimulation of QAQ-treated as described previously (Polosukhina et al., 2012; Tochitsky et al., 2014). A typical MEA protocol consisted of ten cycles of alternating 15 s light and dark intervals. Native light sensitivity was measured with ten cycles of alternating 50 ms light and 15s dark. Spontaneous firing rate in the dark was measured as the average firing of the dark intervals. The Photoswitch Index (PI) was established for individual retinas in 380 nm/500 nm. PI = (mean firing rate in 380 nm light - mean firing rate in 500 nm light) / (mean firing rate in 380 nm light + mean firing rate in 500 nm light).

Patch-clamp recordings were made with a MultiClamp 700B amplifier (Molecular Devices). Cell-attached recordings were performed under voltage clamp at −60 mV, and excitatory

post-synaptic currents were recorded from RGCs, in saline and following perfusion (10 minutes) with a solution containing a mixture of neurotransmitter receptor blockers, as mentioned above. Data were acquired using pCLAMP 10.4 and analyzed with ClampFit 10.5 (Molecular Devices).

Dye loading assay and immunolabeling

Yo-Pro-1 loading in live tissue: After dissection, retinas were cut into thirds and flat-mounted on a windowed nitrocellulose filter paper. Retinas were treated with 200 nM Yo-Pro-1 (Life Technologies) in oxygenated saline for 15 minutes, followed by staining with nuclear ID (Enzo Life Sciences) at a 1:500 dilution for 3 minutes. Saline was perfused continuously at 3 ml/min for a period of 5 minutes to wash away excess dye. In experiments employing TNP-ATP (100 μM), the retinas were pretreated with the compound for 10 minutes before beginning Yo-Pro-1 treatment.

NucFix loading and immunolabeling: NucFix (Biotium) was prepared at a 1:1000 dilution in physiological saline. NucFix labeling was carried out with the same procedure as with Yo-Pro-1 labeling, in living tissue. For co-labeling with antibodies, NucFix-loaded retinal pieces were fixed in 4% paraformaldehyde, blocked using 3% bovine serum albumin and 1:1000 diluted goat anti-mouse IgG (Jackson ImmunoResearch). After rinsing with saline, the tissue was then incubated overnight with monoclonal anti-GFAP-AF488 (GA5, #53–9892-82, Invitrogen) antibody, washed and mounted on glass slides with DAPI-Fluoromount G (Southern Biotech). All procedures were carried out in the dark.

RAR-reporter virus assay

In vitro: HEK293T cells were grown on poly-lysine (Sigma)-coated glass coverslips in 24-well plates (Nunc), in serum-free media to avoid vitamin A. When cultures reached ~70% confluency, they were transfected with the RAR-reporter plasmid using Lipofectamine 2000 (Thermo Fisher). 48 hrs post-transfection, cells were checked for RFP expression, and then treated with ATRA or vehicle (1 % DMSO) for 48 hrs. Cells were then fixed using 4% paraformaldehyde and mounted on glass slides using DAPI-Fluoromont G (Southern Biotech) for imaging.

In vivo: RAR-reporter injected mice and rats, were sacrificed and enucleated. Retinas were isolated as previously described. Whole retinas were partially sectioned on their periphery, making cuts with a scalpel on four symmetrical sides radial to the optic nerve. Whole retinas were flat-mounted onto transparent PDFA membranes (Millipore) and placed on a saline bath. During imaging, retinas were continuously perfused with oxygenated saline.

TUNEL assay—TUNEL assay (In Situ Cell Death Detection Kit, Roche) was carried out in retinas collected 5–6 days following injection with vehicle, ATRA, or ATRA and liarozole. Retinas were fixed inside the cup using 4% paraformaldehyde and embedded in tissue freezing medium. The tissue was cut in 14 μm thick cross-sections using a Leica cryostat.

Imaging

Confocal microscopy: Yo-Pro-1 loading and RAR-reporter virus were imaged using a spinning disk confocal microscope (Olympus BX61WI). The excitation source was a mercury lamp, and fluorescence was collected by a 40x water-immersion objective and standard GFP (488/519 nm) and RFP (561/575 nm) filter cubes (Olympus, U-URA). 1.5 μm section Z-stacks were acquired using a Hamamatsu ImageEM CCD C9100–13.

Image analysis: Images were analyzed with ImageJ or Fiji software (NIH) (Schindelin et al., 2012; Schneider et al., 2012). For the Yo-Pro-1 loading assay, we used nuclear-ID to reveal all nuclei within the GCL and selected regions of interest (ROIs) corresponding to individual non-overlapping nuclei. Overlapping nuclei were excluded, as were those belonging to vascular pericytes, which were associated with blood vessels and had an elongated aspect ratio (>3:2). ROI selection was performed after computationally flattening the retina by employing a maximum Z projection onto a single plane. Background was subtracted using a rolling radius of 50 pixels. A threshold for Yo-Pro-1 loading was established by measuring the level of autofluorescence of untreated retinas in each fluorescence emission channel and finding a baseline mean value and adding 2-standard deviations. Nuclear I.D. (Enzo Life Sciences) was used to count the total number of cells within a field of view. The percentage of cells above the threshold was then calculated for comparison. For analysis of RAR-reporter virus assay, ROIs were manually selected on the RFP channel first and then superimposed onto the GFP channel. Single cell values for both RFP and GFP were filtered by using a RFP minimum threshold established in naive unlabeled retinas.

Behavioral assays

Innate light aversion: Innate light aversion was tested using a light/dark box (Harvard Apparatus, Coulbourn Instruments, H10–24). For the first two days, mice were habituated in the dark to the test room for 2 hrs/day, and on the third day they were habituated in the dark to the box for ~20 minutes. The day of the test, mice were dark adapted for at least 1 hour, then placed in the box in the dark and their activity recorded for 10 minutes. Light was delivered to one side of the box using a single blue LED lamp. Aversion to light was tested at an intensity of ~250 μW/cm^2 for 10 minutes, and ~2500 μW/cm^2 for another 10 minutes (intensity measured ~25 cm from light source). Automated data was generated by infrared sensors on both chambers, recorded and analyzed using Graphic State software (Coulbourn Instruments). The test box was thoroughly cleaned in between mice using 10% bleach.

Learned light aversion: Learned light aversion was tested using a shock-box (Harvard Apparatus, Habitest), containing a shock-delivery grid, a recording camera, and a custom-built panel of three individual LED white lamps coupled to a manual dimmer.

Two days prior to the test, light-adapted mice were individually habituated to the box for 10 minutes. A day before the test, mice were introduced into the chamber for 10 minutes, and were exposed to three consecutive conditioning stimuli, each of them consisting of a 10 seconds-long light pulse (~6000 pW/cm^2) coupled with a 2 seconds-long electric shock (0.5–0.8 mA). The third day, mice were placed in the box for 11 minutes, during which they

were exposed to 4 light stimuli, each 30 seconds-long interspaced by 2 minutes of darkness. The light intensity was incremented between each stimulus. Recordings and analysis was performed by FreezeFrame (Coulbourn Instruments).

Semi-quantitative RT-PCR—Semi-quantitative reverse transcription PCR was employed to assess relative transcription of target genes. Retinas were dissected and immediately homogenized (for each mouse, both retinas were pulled together). RNA was extracted and purified using RNAeasy Kit (Qiagen). cDNA was obtained by reverse transcribing 500 ng of RNA, using SuperScript III Kit (Thermo-Fisher). Semi-quantitative PCR reactions were carried out using AccuPower PCR Pre-Mix tubes (Bioneer), including 0.5 μM primer mix. Analysis of gene expression was conducted using ImageJ to determine mean gray value of gel bands (densitometry).

QUANTIFICATION AND STATISTICAL ANALYSIS

If not stated otherwise, the central tendency is shown as the mean. Variability was calculated as standard error of the mean (SEM). Unless otherwise specified, error bars represent SEM. In all cases, measurements were taken from distinct samples. The Thompson-Tau method was employed for the detection of outliers. If found, outliers were excluded from measurement and statistical analysis. For every comparison between two datasets, a normality Shapiro-Wilk test and, when needed, an Equal Variance test was performed. The specific statistical test for significance performed for each experiment is stated in its corresponding result description and figure legend. If not specified otherwise, Student's t-tests and ANOVA tests were 1-tailed. Pairwise comparisons for non-parametric data employed the Wilcoxon Rank Sum Test. In the case where ANOVA was employed, bootstrapping was used to account for unequal group sizes, a Tukey HSD test was employed as a post-hoc test to define which comparisons and interactions produced statistically significant changes. Results with $p<0.05$ were considered significant. Symbols for p values were used as follows: *<0.05, **<0.01, ***<0.001. See Table S1 for full datasets, sample sizes, statistical tests employed and p values for all comparisons.

DATA AND SOFTWARE AVAILABILITY

The data that support the findings of this study are available from the corresponding author upon request. Table S1 includes full datasets included in the present study.

Supplementary Material

Refer to Web version on PubMed Central for supplementary material.

Acknowledgments:

References

Aggarwal S, Kim SW, Cheon K, Tabassam FH, Yoon JH, and Koo JS (2006). Nonclassical action of retinoic acid on the activation of the cAMP response element-binding protein in normal human bronchial epithelial cells. Molecular biology of the cell 17, 566–575. [PubMed: 16280361]

Anderson EE, Greferath U, and Fletcher EL (2016). Changes in morphology ofretinal ganglion cells with eccentricity in retinal degeneration. Cell and tissue research 364, 263–271. [PubMed: 26670589]

Balmer JE, and Blomhoff R (2002). Gene expression regulation by retinoic acid. Journal of lipid research 43, 1773–1808. [PubMed: 12401878]

Barrett JM, Degenaar P, and Sernagor E (2015). Blockade of pathological retinal ganglion cell hyperactivity improves optogenetically evoked light responses in rdl mice. Frontiers in cellular neuroscience 9, 330. [PubMed: 26379501]

Benbrook DM, Chambón P, Rochette-Egly C, and Asson-Batres MA (2014). History of retinoic acid receptors. Sub-cellular biochemistry 70, 1–20. [PubMed: 24962878]

Bi A, Cui J, Ma YP, Olshevskaya E, Pu M, Dizhoor AM, and Pan ZH (2006). Ectopic expression of a microbial-type rhodopsin restores visual responses in mice with photoreceptor degeneration. Neuron 50, 23–33. [PubMed: 16600853]

Borowska J, Trenholm S, and Awatramani GB (2011). An intrinsic neural oscillator in the degenerating mouse retina. The Journal of neuroscience : the official journal of the Society for Neuroscience 31, 5000–5012. [PubMed: 21451038]

Browne LE, Compan V, Bragg L, and North RA (2013). P2X7 receptor channels allow direct permeation of nanometer-sized dyes. The Journal of neuroscience : the official journal of the Society for Neuroscience 33, 3557–3566. [PubMed: 23426683]

Busskamp V, Duebel J, Balya D, Fradot M, Viney TJ, Siegert S, Groner AC, Cabuy E, Forster V, Seeliger M, et al. (2010). Genetic reactivation of cone photoreceptors restores visual responses in retinitis pigmentosa. Science 329, 413–417. [PubMed: 20576849]

Byrne LC, Lin YJ, Lee T, Schaffer DV, and Flannery JG (2015). The expression pattern of systemically injected AAV9 in the developing mouse retina is determined by age. Molecular therapy : the journal of the American Society of Gene Therapy 23, 290–296. [PubMed: 25224467]

Cehajic-Kapetanovic J, Le Goff MM, Allen A, Lucas RJ, and Bishop PN (2011). Glycosidic enzymes enhance retinal transduction following intravitreal delivery of AAV2. Molecular vision 17, 1771–1783. [PubMed: 21750604]

Chen L, Lau AG, and Sarti F (2014). Synaptic retinoic acid signaling and homeostatic synaptic plasticity. Neuropharmacology 78, 3–12. [PubMed: 23270606]

Choi H, Zhang L, Cembrowski MS, Sabottke CF, Markowitz AL, Butts DA, Kath WL, Singer JH, and Riecke H (2014). Intrinsic bursting of All amacrine cells underlies oscillations in the rdl mouse retina. Journal of neurophysiology 112, 1491–1504. [PubMed: 25008417]

Chute JP, Muramoto GG, Whitesides J, Colvin M, Safi R, Chao NJ, and McDonnell DP (2006). Inhibition of aldehyde dehydrogenase and retinoid signaling induces the expansion of human hematopoietic stem cells. Proceedings of the National Academy of Sciences of the United States of America 103, 11707–11712. [PubMed: 16857736]

Coblentz FE, Radeke MJ, Lewis GP, and Fisher SK (2003). Evidencethat ganglion cells react to retinal detachment. Experimental eye research 76, 333–342. [PubMed: 12573662]

Conlon RA, and Rossant J (1992). Exogenous retinoic acid rapidly induces anterior ectopic expression of murine Hox-2 genes in vivo. Development 116, 357–368. [PubMed: 1363087]

Dagnelie G, Christopher P, Arditi A, da Cruz L, Duncan JL, Ho AC, Olmos de Koo LC, Sahel JA, Stanga PE, Thumann G, et al. (2017). Performance of real-world functional vision tasks by blind subjects improves after implantation with the Argus(R) II retinal prosthesis system. Clinical & experimental ophthalmology 45, 152–159. [PubMed: 27495262]

Damm K, Heyman RA, Umesono K, and Evans RM (1993). Functional inhibition of retinoic acid response by dominant negative retinoic acid receptor mutants. Proceedings ofthe National Academy of Sciences ofthe United States of America 90, 2989–2993.

de The H, Vivanco-Ruiz MM, Tiollais P, Stunnenberg H, and Dejean A (1990). Identification of a retinoic acid responsive element in the retinoic acid receptor beta gene. Nature 343, 177–180. [PubMed: 2153268]

De Voider AG, Bol A, Blin J, Robert A, Arno P, Grandin C, Michel C, and Veraart C (1997). Brain energy metabolism in early blind subjects: neural activity in the visual cortex. Brain research 750, 235–244. [PubMed: 9098549]

Delbeke J, Pins D, Michaux G, Wanet-Defalque MC, Parrini S, and Veraart C (2001). Electrical stimulation of anterior visual pathways in retinitis pigmentosa. Investigative ophthalmology & visual science 42, 291–297. [PubMed: 11133881]

Duester G (2008). Retinoic acid synthesis and signaling during early organogenesis. Cell 134, 921–931. [PubMed: 18805086]

Eleftheriou CG, Cehajic-Kapetanovic J, Martial FP, Milosavljevic N, Bedford RA, and Lucas RJ (2017). Meclofenamic acid improves the signal to noise ratio for visual responses produced by ectopic expression of human rod opsin. Molecularvision 23, 334–345.

Fischer AJ, Wallman J, Mertz JR, and Stell WK (1999). Localization of retinoid binding proteins, retinoid receptors, and retinaldehyde dehydrogenase in the chick eye. Journal of neurocytology 28, 597–609. [PubMed: 10800207]

Germain P, Chambón P, Eichele G, Evans RM, Lazar MA, Leid M, De Lera AR, Lotan R, Mangelsdorf DJ, and Gronemeyer H (2006). International Union of Pharmacology. LX. Retinoic acid receptors. Pharmacological reviews 58, 712–725. [PubMed: 17132850]

Germain P, Gaudon C, Pogenberg V, Sanglier S, Van Dorsselaer A, Royer CA, Lazar MA, Bourguet W, and Gronemeyer H (2009). Differential action on coregulator interaction defines inverse retinoid agonists and neutral antagonists. Chemistry & biology 16, 479–489. [PubMed: 19477412]

Green ES, Menz MD, LaVail MM, and Flannery JG (2000). Characterization of rhodopsin missorting and constitutive activation in a transgenic rat model of retinitis pigmentosa. Investigative ophthalmology & visual science 41, 1546–1553. [PubMed: 10798675]

Harper AR, Wiechmann AF, Moiseyev G, Ma JX, and Summers JA (2015). Identification of active retinaldehyde dehydrogenase isoforms in the postnatal human eye. PloS one 10, e0122008. [PubMed: 25793304]

Harris MA, Clark J, Ireland A, Lomax J, Ashburner M, Foulger R, Eilbeck K, Lewis S, Marshall B, Mungall C, et al. (2004). The Gene Ontology (GO) database and informatics resource. Nucleic acids research 32, D258–261. [PubMed: 14681407]

Hoffman LM, Garcha K, Karamboulas K, Cowan MF, Drysdale LM, Horton WA, and Underhill TM (2006). BMP action in skeletogenesis involves attenuation of retinoid signaling. The Journal of cell biology 174, 101–113. [PubMed: 16818722]

Humayun MS, Dorn JD, da Cruz L, Dagnelie G, Sahel JA, Stanga PE, Cideciyan AV, Duncan JL, Eliott D, Filley E, et al. (2012). Interim results from the international trial of Second Sight's visual prosthesis. Ophthalmology 119, 779–788. [PubMed: 22244176]

Humphries MM, Rancourt D, Farrar GJ, Kenna P, Hazel M, Bush RA, Sieving PA, Shells DM, McNally N, Creighton P, et al. (1997). Retinopathy induced in mice by targeted disruption ofthe rhodopsin gene. Nature genetics 15, 216–219. [PubMed: 9020854]

Innocenti B, Pfeiffer S, Zrenner E, Kohler K, and Guenther E (2004). ATP-induced non-neuronal cell permeabilization in the rat inner retina. The Journal of neuroscience : the official journal of the Society for Neuroscience 24, 8577–8583. [PubMed: 15456831]

Ivanova E, Yee CW, Baldoni R Jr., and Sagdullaev BT (2016). Aberrant activity in retinal degeneration impairs central visual processing and relies on Cx36-containing gap junctions. Experimental eye research 150, 81–89. [PubMed: 26005040]

Janssen JJ, Kuhlmann ED, van Vugt AH, Winkens HJ, Janssen BP, Deutman AF, and Driessen CA (1999). Retinoic acid receptors and retinoid X receptors in the mature retina: subtype determination and cellular distribution. Current eye research 19, 338–347. [PubMed: 10520230]

Jones BW, Pfeiffer RL, Ferrell WD, Watt CB, Marmor M, and Marc RE (2016). Retinal remodeling in human retinitis pigmentosa. Experimental eye research 150, 149–165. [PubMed: 27020758]

Kam RK, Deng Y, Chen Y, and Zhao H (2012). Retinoic acid synthesis and functions in early embryonic development. Cell & bioscience 2, 11. [PubMed: 22439772]

Lin Y, Jones BW, Liu A, Tucker JF, Rapp K, Luo L, Baehr W, Bernstein PS, Watt CB, Yang JH, et al. (2012). Retinoid receptors trigger neuritogenesis in retinal degenerations. FASEBjournal: official publication of the Federation of American Societies for Experimental Biology 26, 81–92.

Maghsoodi B, Poon MM, Nam CI, Aoto J, Ting P, and Chen L (2008). Retinoic acid regulates RARalpha-mediated control of translation in dendritic RNA granules during homeostatic synaptic plasticity. Proceedings of the National Academy of Sciences of the United States ofAmerica 105, 16015–16020.

Marc RE, and Jones BW (2003). Retinal remodeling in inherited photoreceptor degenerations. Molecular neurobiology 28, 139–147. [PubMed: 14576452]

Marc RE, Jones BW, Watt CB, and Strettoi E (2003). Neural remodeling in retinal degeneration. Progress in retinal and eye research 22, 607–655. [PubMed: 12892644]

Margolis DJ, Newkirk G, Euler T, and Detwiler PB (2008). Functional stability of retinal ganglion cells after degeneration-induced changes in synaptic input. The Journal of neuroscience : the official journal of the Society for Neuroscience 28, 6526–6536. [PubMed: 18562624]

Martin KR, Klein RL, and Quigley HA (2002). Gene delivery to the eye using adeno-associated viral vectors. Methods 28, 267–275. [PubMed: 12413426]

Mazzoni F, Novelli E, and Strettoi E (2008). Retinal ganglion cells survive and maintain normal dendritic morphology in a mouse model of inherited photoreceptor degeneration. The Journal of neuroscience : the official journal of the Society for Neuroscience 28, 14282–14292. [PubMed: 19109509]

McCaffery P, Lee MO, Wagner MA, Sladek NE, and Drager UC (1992). Asymmetrical retinoic acid synthesis in the dorsoventral axis of the retina. Development 115, 371–382. [PubMed: 1425331]

McCaffery P, Zhang J, and Crandall JE (2006). Retinoic acid signaling and function in the adult hippocampus. Journal of neurobiology 66, 780–791. [PubMed: 16688774]

Medeiros NE, and Curcio CA (2001). Preservation of ganglion cell layer neurons in age-related macular degeneration. Investigative ophthalmology & visual science 42, 795–803. [PubMed: 11222543]

Mey J, and McCaffery P (2004). Retinoic acid signaling in the nervous system of adult vertebrates. The Neuroscientist: a review journal bringing neurobiology, neurology and psychiatry 10, 409–421.

Middleton JW, Kiritani T, Pedersen C, Turner JG, Shepherd GM, and Tzounopoulos T (2011). Mice with behavioral evidence of tinnitus exhibit dorsal cochlear nucleus hyperactivity because of decreased GABAergic inhibition. Proceedings of the National Academy of Sciences of the United States of America 108, 7601–7606. [PubMed: 21502491]

Milam AH, Li ZY, and Fariss RN (1998). Histopathology ofthe human retina in retinitis pigmentosa. Progress in retinal and eye research 17, 175–205. [PubMed: 9695792]

Mori M, Ghyselinck NB, Chambón P, and Mark M (2001). Systematic immunolocalization of retinoid receptors in developing and adult mouse eyes. Investigative ophthalmology & visual science 42, 1312–1318. [PubMed: 11328745]

Mourot A, Fehrentz T, Le Feuvre Y, Smith CM, Herold C, Dalkara D, Nagy F,Trauner D, and Kramer RH (2012). Rapid optical control of nociception with an ion-channel photoswitch. Nature methods 9, 396–402. [PubMed: 22343342]

Mourot A, Kienzier MA, Banghart MR, Fehrentz T, Huber FM, Stein M, Kramer RH, and Trauner D (2011). Tuning photochromic ion channel blockers. ACS chemical neuroscience 2, 536–543. [PubMed: 22860175]

Mullins RF, Kuehn MH, Radu RA, Enriquez GS, East JS, Schindler EI, Travis GH, and Stone EM (2012). Autosomal recessive retinitis pigmentosa due to ABCA4 mutations: clinical, pathologic, and molecular characterization. Investigative ophthalmology & visual science 53, 1883–1894. [PubMed: 22395892]

Novitch BG, Wichterle H, Jessell TM, and Sockanathan S (2003). A requirement for retinoic acid-mediated transcriptional activation in ventral neural patterning and motor neuron specification. Neuron 40, 81–95. [PubMed: 14527435]

O'Brien EE, Greferath U, and Fletcher EL (2014). The effect of photoreceptor degeneration on ganglion cell morphology. The Journal of comparative neurology 522, 1155–1170. [PubMed: 24519018]

Parker RO, and Crouch RK (2010). Retinol dehydrogenases (RDHs) in the visual cycle. Experimental eye research 91, 788–792. [PubMed: 20801113]

Phillips MJ, Otteson DC, and Sherry DM (2010). Progression of neuronal and synaptic remodeling in the rdlO mouse model of retinitis pigmentosa. The Journal of comparative neurology 518, 2071–2089. [PubMed: 20394059]

Polosukhina A, Litt J, Tochitsky I, Nemargut J, Sychev Y, De Kouchkovsky I, Huang T, Borges K, Trauner D, Van Gelder RN, et al. (2012). Photochemical restoration of visual responses in blind mice. Neuron 75, 271–282. [PubMed: 22841312]

Porciatti V (2015). Electrophysiological assessment of retinal ganglion cell function. Experimental eye research 141, 164–170. [PubMed: 25998495]

Russo JE, Hauguitz D, and Hilton J (1988). Inhibition of mouse cytosolic aldehyde dehydrogenase by 4-(diethylamino)benzaldehyde. Biochemical pharmacology 37, 1639–1642. [PubMed: 3358794]

Schindelin J, Arganda-Carreras I, Frise E, Kaynig V, Longair M, Pietzsch T, Preibisch S, Rueden C, Saalfeld S, Schmid B, et al. (2012). Fiji: an open-source platform for biological-image analysis. Nature methods 9, 676–682. [PubMed: 22743772]

Schneider CA, Rasband WS, and Eliceiri KW (2012). NIH Image to ImageJ: 25 years of image analysis. Nature methods 9, 671–675. [PubMed: 22930834]

Sekirnjak C, Jepson LH, Hottowy P, Sher A, Dabrowski W, Litke AM, and Chichilnisky EJ (2011). Changes in physiological properties of rat ganglion cells during retinal degeneration. Journal of neurophysiology 105, 2560–2571. [PubMed: 21389304]

Stasheff SF (2008). Emergence of sustained spontaneous hyperactivity and temporary preservation of OFF responses in ganglion cells of the retinal degeneration (rdl) mouse. Journal of neurophysiology 99, 1408–1421. [PubMed: 18216234]

Stasheff SF, Shankar M, and Andrews MP (2011). Developmental time course distinguishes changes in spontaneous and light-evoked retinal ganglion cell activity in rdl and rdlO mice. Journal of neurophysiology 105, 3002–3009. [PubMed: 21389300]

Stronks HC, and Dagnelie G (2014). The functional performance of the Argus II retinal prosthesis. Expert review of medical devices 11, 23–30. [PubMed: 24308734]

Tochitsky I, Helft Z, Meseguer V, Fletcher RB, Vessey KA, Telias M, Denlinger B, Malis J, Fletcher EL, and Kramer RH (2016). How Azobenzene Photoswitches Restore Visual Responses tothe Blind Retina. Neuron 92, 100–113. [PubMed: 27667006]

Tochitsky I, Kienzier MA, Isacoff E, and Kramer RH (2018). Restoring Vision to the Blind with Chemical Photoswitches. Chemical reviews.

Tochitsky I, Polosukhina A, Degtyar VE, Gallerani N, Smith CM, Friedman A, Van Gelder RN, Trauner D, Käufer D, and Kramer RH (2014). Restoring visual function to blind mice with a photoswitch that exploits electrophysiological remodeling of retinal ganglion cells. Neuron 81, 800–813. [PubMed: 24559673]

Toychiev AH, Ivanova E, Yee CW, and Sagdullaev BT (2013). Block of gap junctions eliminates aberrant activity and restores light responses during retinal degeneration. The Journal of neuroscience : the official journal of the Society for Neuroscience 33, 13972–13977. [PubMed: 23986234]

Trapani I, and Auricchio A (2018). Seeing the Light after 25 Years of Retinal Gene Therapy. Trends in molecular medicine 24, 669–681. [PubMed: 29983335]

Trenholm S, Borowska J, Zhang J, Hoggarth A, Johnson K, Barnes S, Lewis TJ, and Awatramani GB (2012). Intrinsic oscillatory activity arising within the electrically coupled All amacrine-ON cone bipolar cell network is driven by voltage-gated Na+ channels. The Journal of physiology 590, 2501–2517. [PubMed: 22393249]

Turrigiano GG (1999). Homeostatic plasticity in neuronal networks: the more things change, the more they stay the same. Trends in neurosciences 22, 221–227. [PubMed: 10322495]

Van Wauwe J, Van Nyen G, Coene MC, Stoppie P, Cools W, Goossens J, Borghgraef P, and Janssen PA (1992). Liarozole, an inhibitor of retinoic acid metabolism, exerts retinoid-mimetic effects in vivo. The Journal of pharmacology and experimental therapeutics 261, 773–779. [PubMed: 1374473]

Virginio C, Mackenzie A, Rassendren FA, North RA, and Surprenant A (1999). Pore dilation of neuronal P2X receptor channels. Nature neuroscience 2, 315–321. [PubMed: 10204537]

Virginio C, Robertson G, Surprenant A, and North RA (1998). Trinitrophenyl-substituted nucleotides are potent antagonists selective for P2X1, P2X3, and heteromeric P2X2/3 receptors. Molecular pharmacology 53, 969–973. [PubMed: 9614197]

Yee CW, Toychiev AH, and Sagdullaev BT (2012). Network deficiency exacerbates impairment in a mouse model of retinal degeneration. Frontiers in systems neuroscience 6, 8. [PubMed: 22383900]

Highlights:

- Photoreceptor degeneration leads to retinal ganglion cell hyperactivity.

- Hyperactivity is triggered by over-production of retinoic acid (RA).

- Blocking the RA receptor with drug or gene therapy reduces hyperactivity.

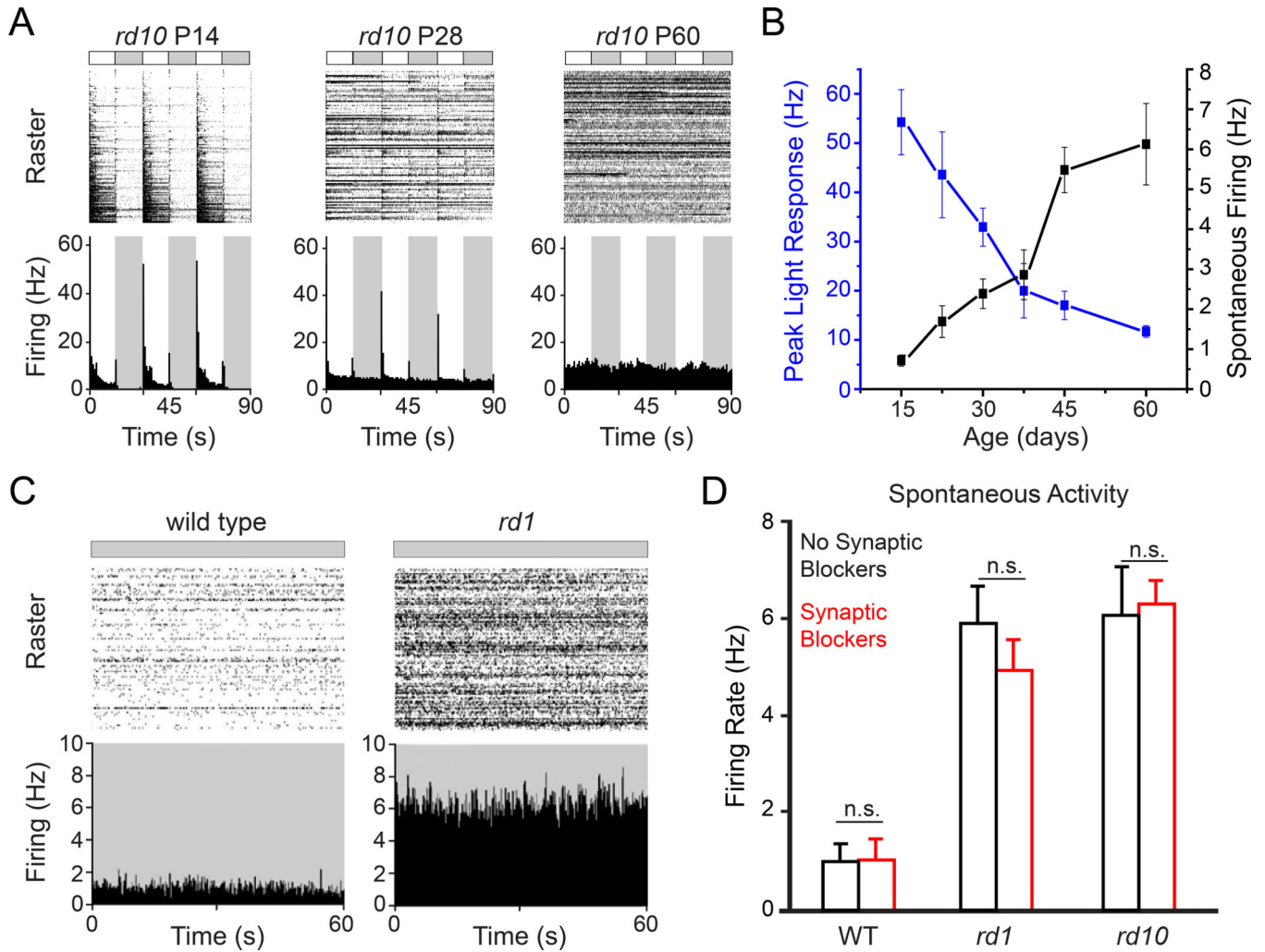- RA receptor blockade augments light-evoked behaviors in vision-impaired mice.

Figure 1. Retinal degeneration induces hyperactivity.

(A) MEA recordings of retinal light responses of *rd10* mice at ages P14, 28 and 60.

(B) Quantification of peak light responses and spontaneous activity in the dark as a function of age in *rd10* mice *ex vivo* retinal pieces. Values are mean ± SEM, measured in 7 – 10 retinal pieces at each age (P14–60).

(C) MEA recordings of spontaneous activity of synaptically-isolated RGCs in the dark in P60 *rd1* retina and in a normal WT counterpart. See also Figure S1.

(D) Spontaneous firing in normal saline (black) and after adding synaptic blockers (red). To eliminate rod-mediated light responses, we promoted bleaching adaptation by exposing the isolated retinas to room light for 30 minutes before recording (Dowling J, 1987). In all three strains synaptic blockade caused no change in spontaneous firing (n.s.: non-significant, WT: n = 9, p = 0.99; *rd1:* n = 6, p = 0.28; *rd10:* n = 4, p = 0.76; paired t-test). Spontaneous firing in *rd1* and *rd10* remained significantly higher than in WT, even after synaptic blockade. Values are mean ± SEM. For full dataset, see Table S1.
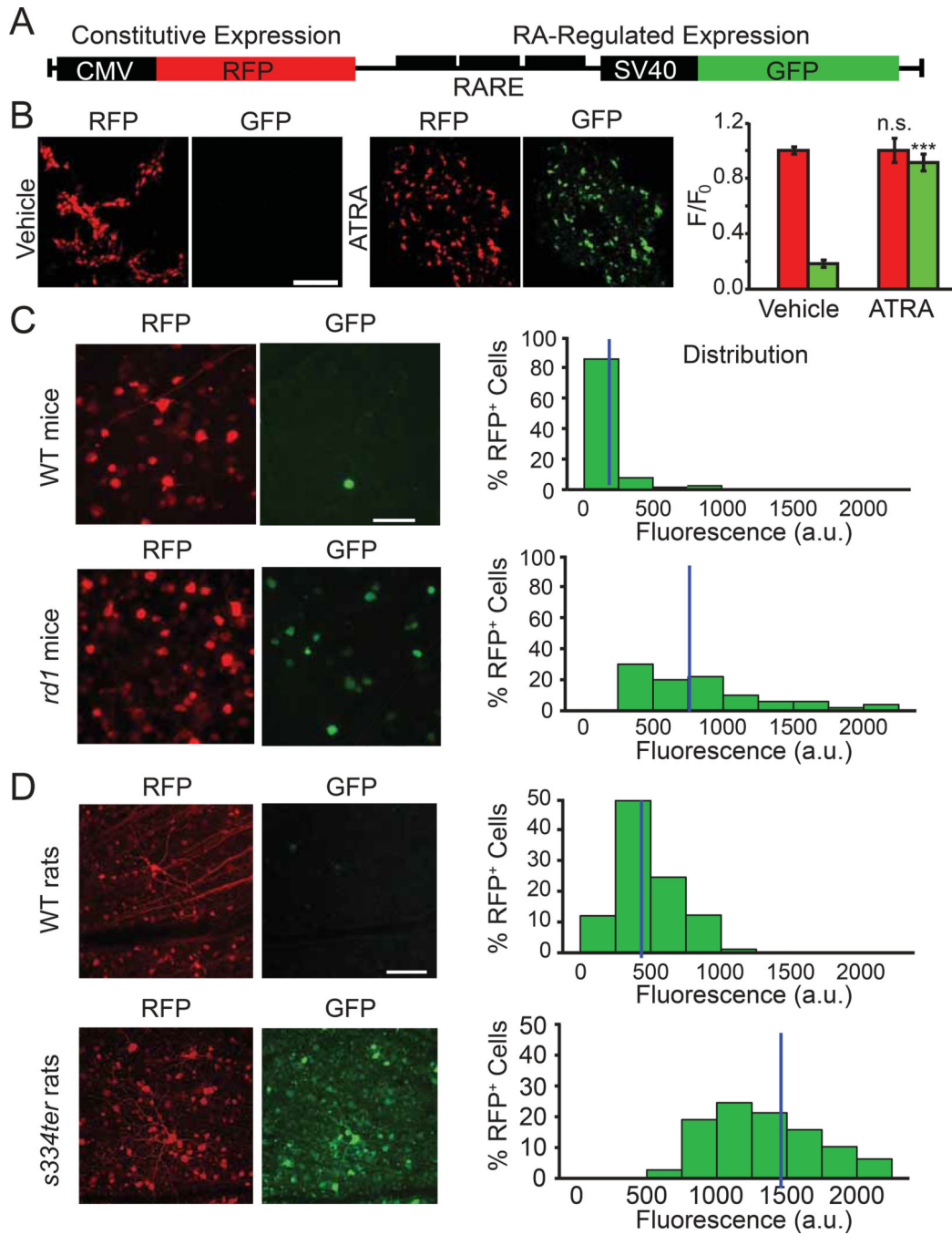
Figure 2. A genetically-encoded RAR-reporter shows increased RAR-signaling *in-vivo*.
(A) Schematic representation of the reporter construct. Red fluorescent protein (RFP) is under control of the cytomegalovirus promoter (CMV) resulting in constitutive expression. Green fluorescent protein (GFP) is under the control of a triple repeat of the Retinoic Acid Response Element (RARE) upstream to a weak SV40 promoter, resulting in RA-regulated expression.

(B) Left: fluorescence images of HEK293 cells expressing the RAR reporter. Cells were lipofectamine-transfected and 48 hrs later, either vehicle alone (0.1% DMSO in PBS) or

with 1 μM *all-trans* retinoic-acid (ATRA) were added to the culture medium for an additional 48 hrs. Images show strong RFP expression after either vehicle or ATRA treatment, but a significant increase in GFP expression only following ATRA treatment. Right: quantification of RFP and GFP fluorescence, normalized to mean RFP fluorescence values in vehicle-treated cells. Values are shown as mean ± SEM, 3 separate experiments were conducted in duplicate wells of HEK cells grown in serum-free media. n.s.: non-significant, ***$p<0.001$,2-tailed t-test. See also Figure S2.

(C,D) The RAR reporter shows RA signaling in the ganglion cell layer (GCL) from WT and degenerated mouse retina *(rd1,* C), and WT and degenerated rat retina *(s334ter,*D). RA-dependent signaling was quantified in individual cells by measuring GFP fluorescence in RFP-expressing cells (mean gray value in arbitrary units, 'a.u.'). Histograms show the distribution of GFP fluorescence in RFP-positive cells. Data for individual cell values were pooled from 8–10 retinas in 4–5 animals per strain. Each retina was divided into 3–4 pieces, and 4–6 fields of view were imaged and analyzed for each piece. Images correspond to 2D projections of Z-stacks from a spinning disk confocal microscope. Blue vertical line indicates the median value of GFP fluorescence for each distribution. Animals were injected intravitreally at P30–45 with AAV2-RAR-reporter and analyzed ~60–90 days later. See also Figure S3. For full datasets, see Table S1.
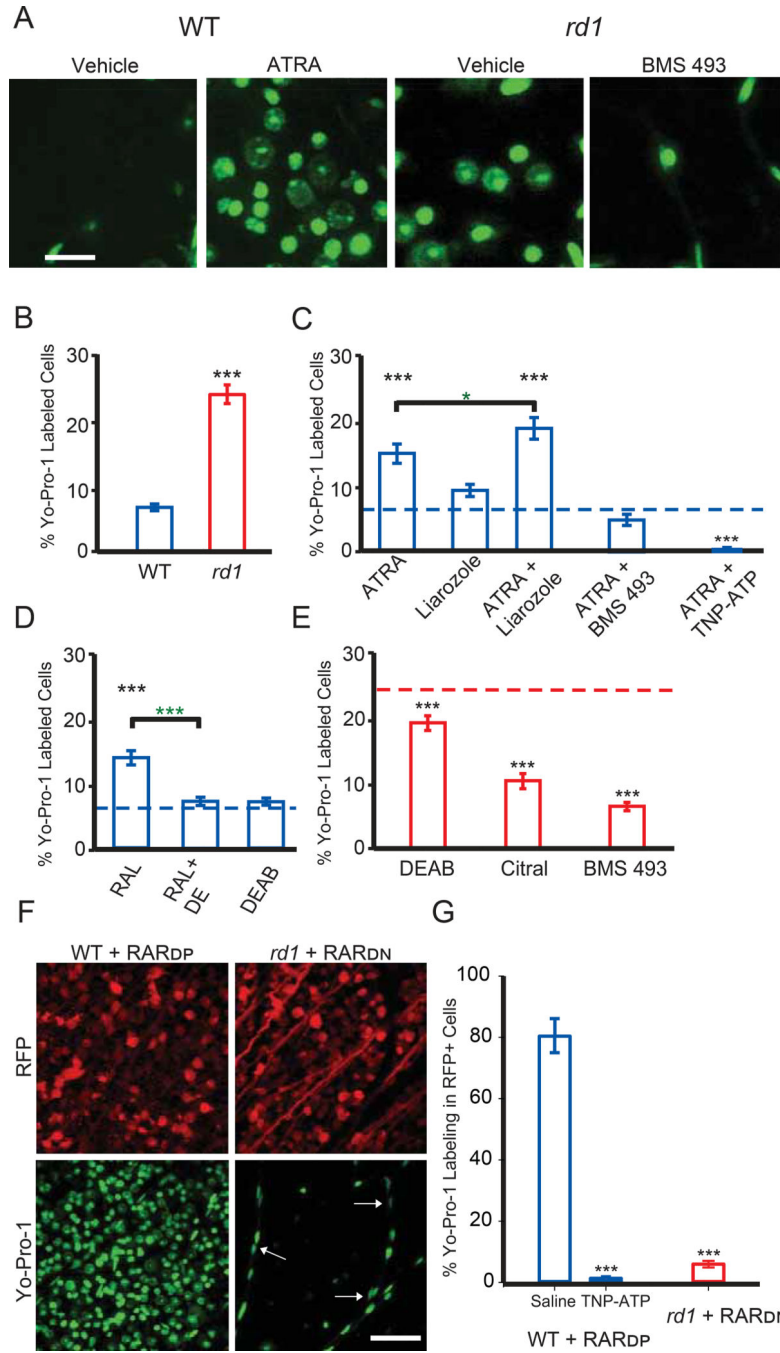
Figure 3. RAR activation induces hyper-permeability of degenerated retinas through P2X receptors.

(A) Images of Yo-Pro-1 (green) labeling of cell nuclei in the ganglion cell layer (GCL) of WT retinas injected with vehicle or ATRA, and in *rd1* retinas injected with vehicle, or RAR inhibitor BMS 493. Scale bar is 20μm in length. Images are a 2D projection of a Z-stack.

(B) Quantification of the fraction of cells labeled with Yo-Pro-1 for vehicle-injected (1 μL intra-vitreous, 1% DMSO in PBS, 3–7 days prior to dye loading assay) in WT and *rd1* retinal pieces (blue and red, respectively). Data are shown as the percentage of Yo-Pro-1 positive cells in a field of view (counterstained with Nuclear I.D., not shown).

(C) Quantification as in (B), above. All experiments were conducted in WT retinas. Intravitreal injections included 0.1 μM *all-trans* retinoic acid (ATRA), 100 μM Liarozole (Cyp26 inhibitor) and 0.5 μM BMS 493 (pan-RAR inverse agonist). 200 μM TNP-ATP (P2X antagonist) was bath loaded. Black asterisks - compared to WT baseline (B, dotted blue line), green asterisks - ATRA vs. ATRA+Liarozole.

(D) Quantification as in B, above. All experiments were conducted in WT retinas. Intravitreal injections included 0.5 μM retinaldehyde (RAL) and 20 μM N,N-diethylaminobenzaldehyde (DEAB, RALDH inhibitor). Black asterisks - compared to WT baseline (B, blue dotted line), green asterisks - RAL vs. RAL+DEAB.

(E) Quantification as in B, above. All experiments were conducted in *rd1* retinas. Intravitreal injections included 20 μM DEAB, 50 μM Citral (RALDH inhibitor), and 0.5 μM BMS 493. Black asterisks - compared to *rd1* baseline (B, red dotted line).

(F) Images of Yo-Pro-1 labeling in the GCL after viral gene therapy to express RAR_{DP} in WT retinas (left) and after viral gene therapy to express RAR_{DN} in *rd1* (right). Virally-infected neurons also express red fluorescent protein (RFP), a co-expression marker. White arrows show pericytes in the vasculature. Scale bar is 50 μm.

(G) Quantification of F, as the fraction of RFP-expressing cells that were positively labeled with Yo-Pro-1.200 μM TNP-ATP (P2X antagonist) was bath applied. (B-E, G) Values are shown as mean ± SEM. *p<0.05, ***p<0.001, t-test and MannWhitney. See also Figures S4, S5 and S6. For full datasets, see Table S1.
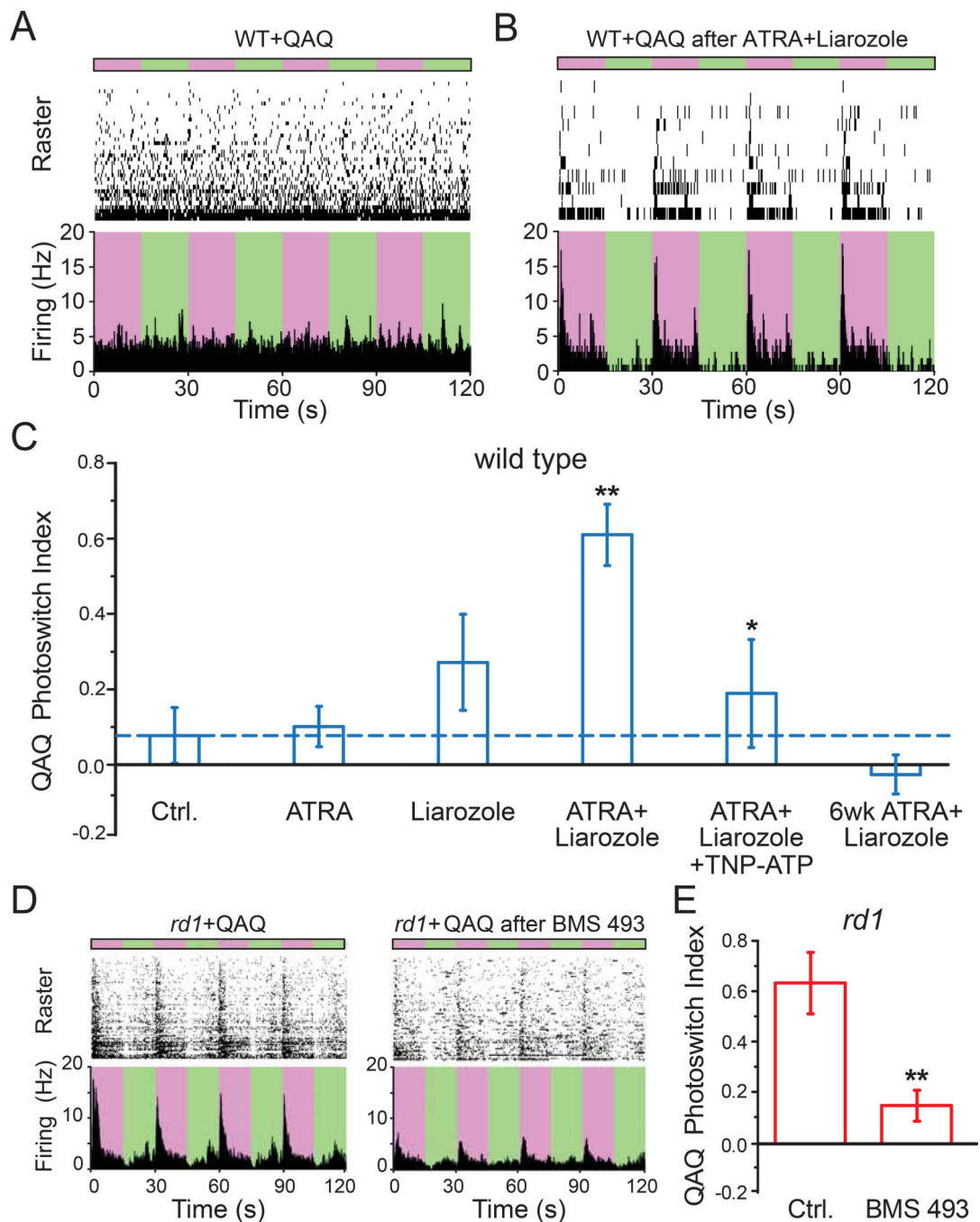
Figure 4. Pharmacological activation of RAR is necessary and sufficient for degeneration-dependent chemical photosensitization.

(A-B) MEA recordings from QAQ-treated WT retina, without (A) or with (B) prior intravitreal injection of ATRA plus liarozole. Photoswitching was elicited by alternating between 380 nm (purple) and 500 nm (green) light. 300 μM QAQ was applied onto the isolated retina for 30 minutes and then washed away.

(C) Quantification of (A-B). Photosensitivity (Photoswitch Index, PI) induced by QAQ was measured in WT retinas (blue). Recordings were obtained 3–7 days after ~1 μl intravitreal injection, including 1% DMSO in PBS (vehicle control, 'Ctrl.', dotted line in blue), 0.1 μM

all-trans retinoic acid (ATRA), 100 μM Liarozole (Cyp26 inhibitor). Recordings were also obtained 6 weeks after injection of ATRA + Liarozole. 200 μM TNP-ATP (P2X antagonist) was bath loaded. ** - Ctrl. vs ATRA + Liarozole, * - ATRA + Liarozole vs ATRA + Liarozole + TNP-ATP.

(D) Blocking RAR reduces QAQ-photosensitization in *rd1* retinas. Retinas were obtained from eyes without (left) or with (right) BMS 493 (0.5 μM), injected into the vitreous at 3–7 days prior to retina isolation and recording.

(E) Quantification of (D) in *rd1* retinas (red). Control ('Ctrl.', non-injected eyes), were compared to rd1 eyes injected with 0.5 μM BMS 493, 3–7 days prior to recordings. (C&E) Values are shown as mean ± SEM. $*p < 0.05$, $**p < 0.01$, Kruskal-Wallis and t-test. For full datasets, see Table S1.
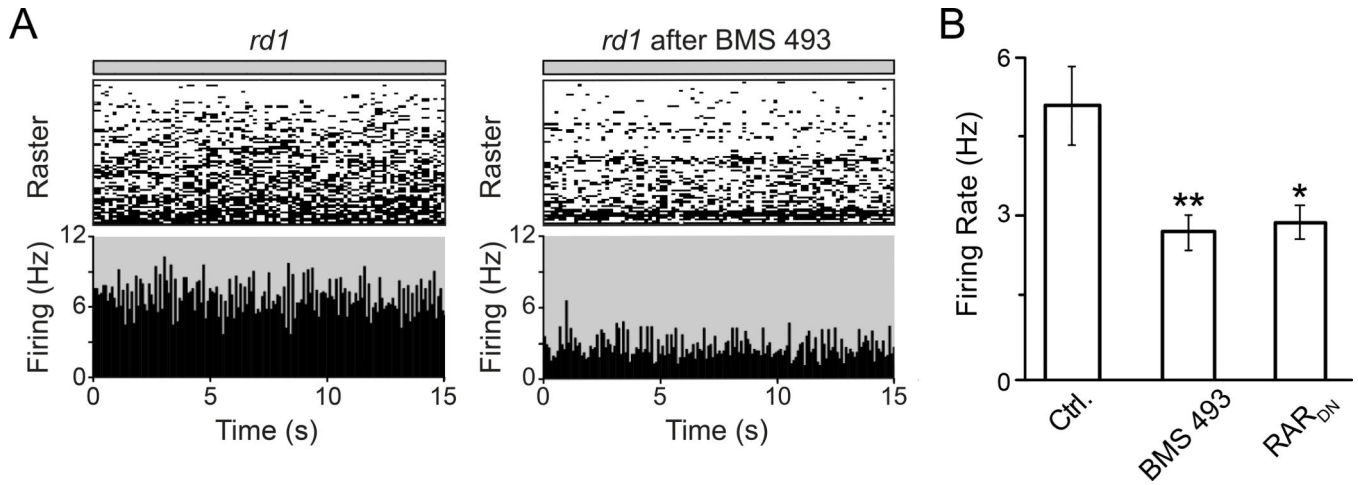
Figure 5. Pharmacological or genetic inhibition of RAR reduces hyperactivity in the degenerated *rd1* retina.

(A) MEA recordings of spontaneous activity in the dark, in a naive *rd1* retina (left), and in a BMS 493-injected *rd1* retina (right), both in saline.

(B) Quantification of spontaneous activity in *rd1* control retinas ('Ctrl.', non-injected eyes), in *rd1* retinas injected with 0.5 μM BMS 493 3–7 days prior to the experiment, and in *rd1* retinas from P90 mice, injected at P30 with AAV2-RAR$_{DN}$. Values represent the mean Firing Rate (Hz) ± SEM. $*p < 0.05$, $**p < 0.01$, one-way ANOVA. For full datasets, see Table S1.
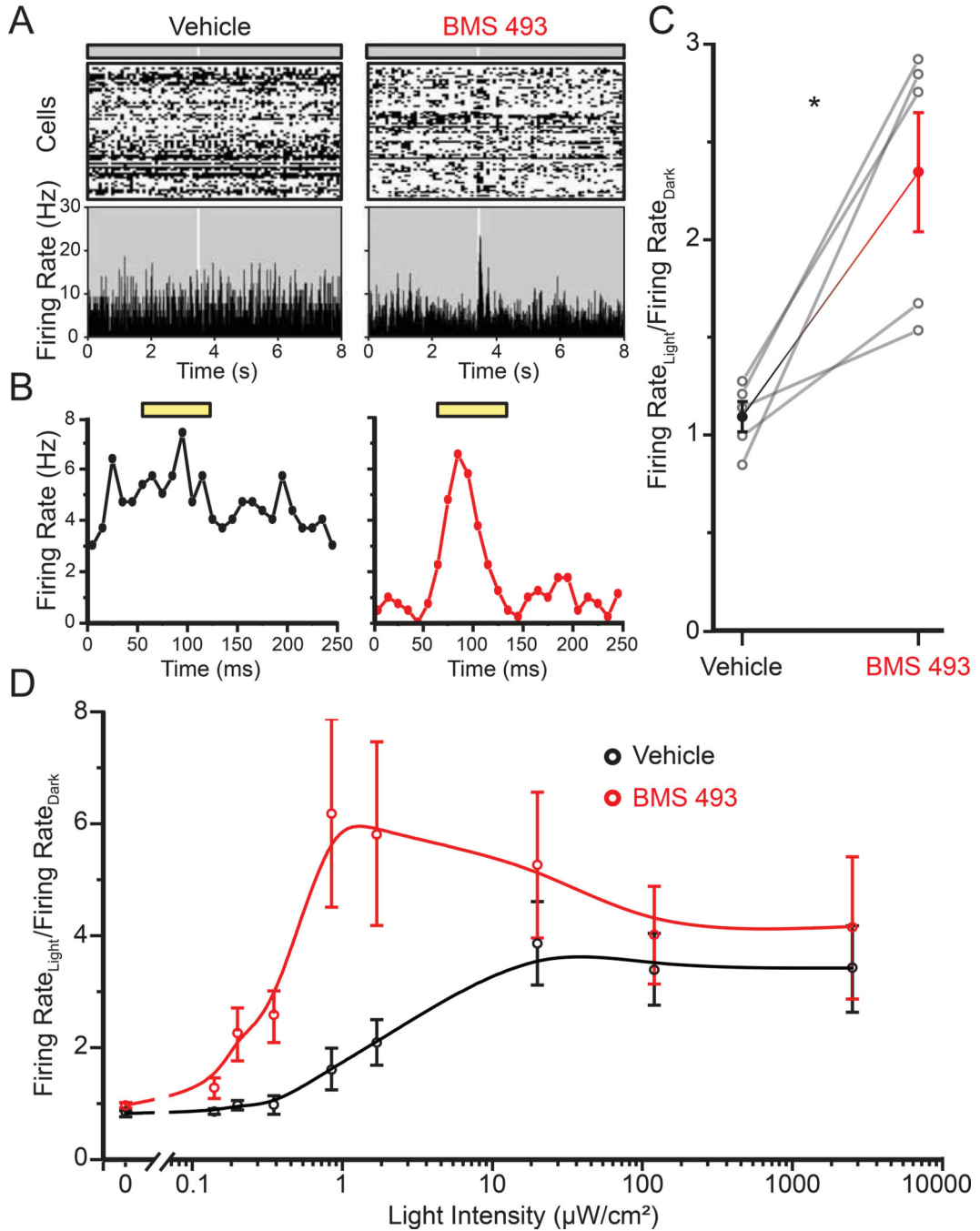
Figure 6. Inhibition of RAR activation reduces hyperactivity of RGCs and boosts light responses in *rd10* vision-impaired mice.

(A) In partially degenerated retinas from P41–43 *rd10* mice, response to a single dim light flash (white light, 50 ms, 0.2 µW) in normal saline, recorded with the MEA. Note the high spontaneous firing rate and lack of a light-response in the retina isolated from the vehicle-injected eye, and the lower spontaneous firing rate and transient light response in the retina from the BMS 493-injected eye. Top shows raster plots of individual RGC activities, bottom shows average firing rate from all cells.

(B) The average of 9 light flashes, showing reduced spontaneous activity and robust light response in the BMS 493-injected eye.

(C) Responses from 5 mice, comparing the light-elicited change in firing in the vehicle-injected (1%DMSO in PBS) and BMS 493-injected eye. Data is shown as mean ± SEM, *p<0.05, Paired t-test.

(D) Intensity-response curves from the retinas of vehicle-injected and BMS 493-injected eyes. Solid line is a basis-spline fit to the data. Data are represented as the mean ratio of firing rate in the light/dark ± SEM. For full dataset, see Table S1.
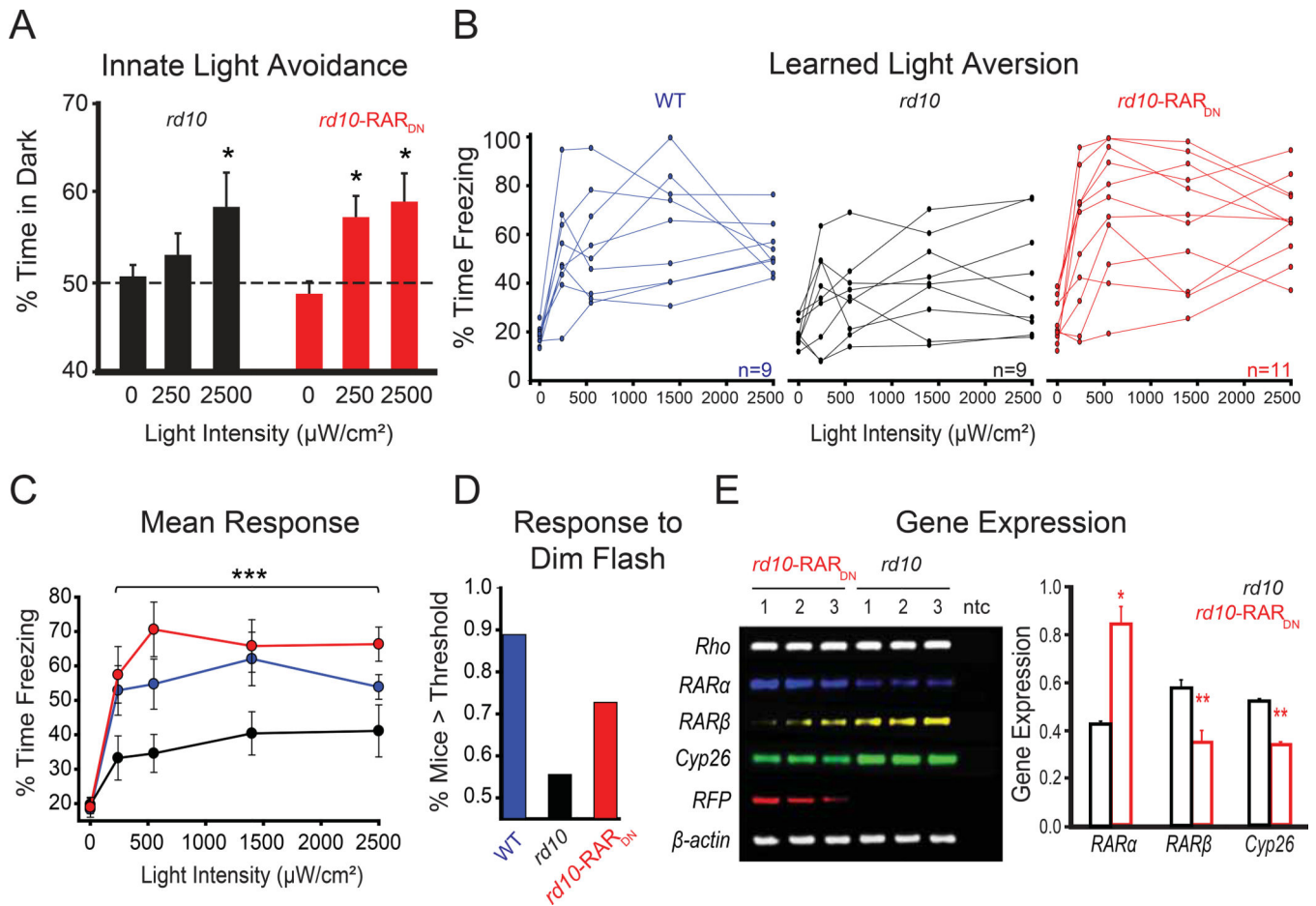
Figure 7. *In vivo* blockade of RAR increases innate and learned visual responses.

(A) Quantification of innate aversion to light in naive *rd10* mice (black bars) as compared to *rd10* mice injected at P2–3 with RAR$_{DN}$ (red bars). All mice were tested at P37–38. The graph shows the % of time spent by the mouse in the dark side of the chamber as a function of light intensity (darkness, ~250 μW/cm^2, 2500 μW/cm^2). Values are mean ± SEM, *p<0.05, X^2-test.

(B) Individual traces for light responses (% time spent freezing) to darkness (0) and four different intensities of light (240, 550, 1400 and 2500 μW/cm^2), using the learned light aversion behavioral paradigm. Untreated WT (blue traces) and *rd10* mice (black traces) were compared to *rd10* mice injected at P2–3 with RAR$_{DN}$ (red traces). All mice were tested at P33–35.

(C) Quantification of B. The graph shows % of time spent freezing as a function of light intensity. Values are mean ± SEM, ***p<0.001, t-test (WT and rd10-RAR$_{DN}$ vs *rd10*).

(D) Probability of mouse displaying a response above threshold for the first light flash using the dimmest intensity (~240 μW/cm^2), in each strain, including WT (blue bar), *rd10* (black bar) and rd10-RAR$_{DN}$ (red bar). For each individual trace in B, the slope of the response was measured, and threshold was set as a slope that is +0.05.

(E) Gel electrophoresis (left) and quantification (right) of semi-quantitative reverse-transcription PCR assay carried out on RNA extracted from retinas of rd10-RAR$_{DN}$ and

naive *rd10* mice. All mice were P40 at the day of dissection and RNA purification. ntc - non-template control; *Rho* - rhodopsin; *RARα* - retinoic acid receptor alpha; *RARβ* - retinoic acid receptor beta; *Cyp26* - cytochrome P450 26A1; *RFP* - red fluorescent protein *(mStrawberry). β-Actin* was used as a housekeeping gene. Quantification of relative transcript levels for gene expression was normalized to *β-actin. rd10* is shown in black and *rd10-RAR*$_{DN}$ in red. Values are mean ± SEM, *p<0.05, **p<0.001, t-test. (A-C, E) For full dataset, see Table S1.